Electrocatalysis for Polymer Electrolyte Fuel Cells: Recent Achievements and Future Challenges

Annett Rabis,[†] Paramaconi Rodriguez,[†] and Thomas J. Schmidt[†,‡,*]

[†]Electrochemistry Laboratory, General Energy Research Department, Paul Scherrer Institut, CH-5232 Villigen, Switzerland
[‡]Laboratory of Physical Chemistry, Electrochemistry Group, ETH Zürich, CH-8093 Zürich, Switzerland

ABSTRACT: Fuel cell technology is currently shifting very fast from fundamental research to real development. In addition to other aspects, this transition is possible because of the important improvements achieved in the field of electrocatalysis in the past decade. This perspective will give a focused overview summarizing the most outstanding contributions in the last 10 years in terms of activity and durability of the catalyst materials for ethanol oxidation and oxygen reduction reaction, respectively. In addition, it provides an outlook about new catalyst support materials with improved performance/ stability, advanced characterization techniques, and fundamental studies of reaction mechanisms and degradation processes. All the studies referred to in this perspective significantly contribute to reaching the technical targets for PEFC commercialization.

KEYWORDS: *electrocatalysis, fuel cell, oxygen reduction reaction, alcohol oxidation*

1. INTRODUCTION AND SCOPE

The commercialization of hydrogen fuel cells is one of the major prerequisites for enabling a sustainable hydrogen-based economy. In this context, low-temperature (LT; operating at −20 to 100 °C) and high-temperature (HT; operating at 100−180 °C) polymer electrolyte fuel cells (PEFCs) are promising and far-developed technologies for automotive and for stationary and small portable applications, respectively. Over the past 30 years, system, stack and stack component development have been carried out in academic, institutional, and industrial environments. Despite these development efforts, performance and durability of the key components, such as membrane electrode assemblies (MEAs), membranes, electrodes, gaskets, or bipolar plates remain the focus of international research and development (R & D).

In PEFCs, electrochemical reactions (e.g., the hydrogen oxidation reaction (HOR)) or alcohol oxidation reactions (AOR, e.g., methanol, ethanol) and oxygen reduction reaction (ORR) take place on the surface of typical Pt-based catalysts at the so-called three-phase boundary. Especially on the cathode side of the PEFC, where the ORR takes place, both the catalyst kinetics and the corrosion stability of the catalyst need to be improved significantly to make PEFCs cost-competitive devices for automotive and stationary applications. In direct alcohol fuel cells (e.g., direct methanol (DMFC) or direct ethanol (DEFC) fuel cells), in addition to the ORR, the oxidation of the fuel is of major interest because of sluggish alcohol oxidation kinetics and the formation of catalyst poisoning intermediates.

In Table 1, the overall goals for automotive applications (performance and durability), small stationary PEFC applica-

tions (mainly durability; performance questions are only critical in correlation to reaching the cost targets), and small fuel cells for consumer electronics are summarized. Although the cost targets for the three mentioned classes of PEFCs are different and highly depend on the final application, reaching these goals goes hand in hand with electrocatalysis questions, since mainly costly precious metal catalysts from the platinum group are used. On the basis of a 2008 study from the International Partnership for Hydrogen and Fuel Cells in the Economy (IPHE),[1] almost 50% of the PEFC stack cost in an automotive fuel cell system is related to the catalysts and their application. A recent 2011 fuel cell system cost analysis for high-volume manufacturing (500 000 units, 80 KW_{net})[2] assumes Pt cost to be only ∼30% of the stack cost, assuming a Pt prize of $35/g (note that the January 2012 prize is more on the order of $50/ g). Nevertheless, despite fluctuating Pt market prizes, it is clear that because of this high share, every increase in reaction kinetics will be directly reflected in reduced stack (and system) cost. It should be mentioned that results from this study estimate an ∼45% share of the stack on the total system cost. With respect to the other systems, specifically small systems for consumer electronics using direct alcohol fuel cells, the percentage of catalyst cost on the total system cost may be significantly higher due to higher amounts of precious metals used.

Table 1. Overall Performance and Durability Goals for Automotive, Small Stationary (1 kW$_e$ to 10 kW$_e$) PEFCs and Direct Alcolhol Fuel Cells for Consumer Electronics (10−50 W)[a]

	current status	goal 2017	comments
		Automotive	
catalyst performance	0.24 A/mg$_{Pt}$ to 0.8 A/mg$_{Pt}$ at 0.9 V[3] 1300 μA/cm$_{Pt}$ to 2700 μA/cm$_{Pt}$ at 0.9 V[3] (2011 status)	>0.44 A/mg$_{Pt}$ at 0.9 V	current status is based on recent results from 3M NSTF catalysts[3] for PtCoMn (lower end of values) and Pt$_3$Ni$_7$ (higher end of values), single cell data
catalyst loading (stack level)	0.15 mg$_{PGM}$/cm$^2_{electrode}$	0.125 mg$_{PGM}$/cm$^2_{electrode}$	PGM: platinum group metals
durability (stack level)	2500 h	>5000 h	under typical drive cycle conditions (up to 40.000 start−stop cycles expected for typical automotive operation), based on U.S. DRIVE Fuel Cell Tech Team Cell Component Accelerated Stress Test and Polarization Curve Protocols[4]
		Stationary 5−10 kW	
durability (system level)	12.000 h	40.000−90.000 h	daily start−stop operation; the values based on DOE and NEDO targets
cost (system level)	$2.300−4.000 /kW (2011 status)	$1.700−1.900 /kW	DOE targets
		Consumer Electronics 10−50 W	
durability (system)	1500 h	5000 h (2015 target)	
system performance	15 W/kg; 20 W/L (2011 status)	45 W/kg; 55 W/L (2015 target)	2011 status $15 /W
anode catalyst performance	200 mA/mg$_{Pt}$ at 0.25 V	200 mA/mg$_{Pt}$ at 0.25 V (2014 project target)[5]	DMFC[5]
cell performance	75 mA/cm^2 at 0.6 V[5]	150 mA/cm^2 at 0.6 V[5]	using 6 mg/cm^2 PtRu black and 4 mg/cm^2 Pt black catalysts

[a]Data summarized from refs 6, 7 (U.S. Department of Energy and Japanese NEDO).

In recent years, many new approaches in fuel cell electrocatalysis have been worked on. Whereas the need for highly durable and efficient electrocatalysts for the ORR and the oxidation of alcohols, respectively, was outlined before from a top-view level, in what follows, we will be detailing our perspective on the status of electrocatalysis in PEFC research and development.

The first part of the manuscript deals with the task of improving catalyst performance for both oxidation of alcohols and oxygen reduction. The kinetic performance of the electrocatalyst for these reactions is crucial, and in-depth understanding of the reactant, reaction intermediates, spectators, and the catalyst surface is of utmost importance to design more active catalysts. The catalytic activity of the different catalyts will be evaluated in terms of current densities (per geometric and specific surface area or per mass) under identical or at least similar operating conditions (although this is not always possible in cross-laboratoy comparisons). As discussed above, the catalyst loading in a fuel cell electrode is directly correlated not only to the fuel cell power density but also to the fuel cell cost. New approaches to improve catalyst kinetics as well as recent developments in the understanding and development of nonprecious metal catalysts will be presented.

Many of these catalyst developments, including the in-depth understanding of reaction mechanisms, was possible through the important breakthrough developments in computational studies, i.e., the application of molecular dynamics, quantum mechanical, and density functional theory (DFT) calculations.[8−18] These studies not only helped for a better understanding but also proved predictive capabilities for novel improved catalysts. In addition to the advanced theoretical tools that have helped to improve electrocatalysts, the progress in the application of new experimental techniques is closely related to electrocatalyst research.

One important step in studying realistic fuel cell catalysts under well-defined electrochemical and mass transport conditions was the development of the thin-film rotating ring-disk electrode (RRDE) technique in 1998.[19−21] Since then, this technique has been copied, modified, and partially improved by many groups working on fuel cell electrocatalysts and has significantly helped the development of new catalyst systems. See the many examples given here in the context of this manuscript. The thin-film RRDE method not only allows for the study of reaction kinetics, it also is widely applied for potential cycling and other catalyst durability measurements.

In addition, many improvements (e.g., of in situ X-ray scattering studies,[22−26] in situ infrared spectroscopy[24,27−30] or online mass-spectrometry[31−33]) are without doubt the origin of both a better understanding of reaction mechanisms and structure−reactivity relationships in electrocatalysis. Especially, in situ small-angle X-ray scattering has proven to be a powerful tool to study structural changes of fuel cell components; for instance, nanoparticles, support materials, or porous media.[34] Recent developments in high-resolution transmission electron microscopy (e.g., scanning TEM etc.) are being used now by many researchers to better understand catalyst morphology and composition and their changes upon the electrochemical reaction (see e.g., refs 35, 36). Especially the development of the so-called identical location TEM has proved to be very well suited for catalyst degradation studies, since it allows the imaging of identical catalyst particles before and after the electrochemical reaction.[37] Similar theoretical and experimental tools and techniques are utilized in the studies of catalyst and electrode lifetime.

Having said that, in addition, large efforts have been made to determine accelerated aging protocols to study catalyst and electrode degradation at conditions relevant to technical fuel cell operation. It should be emphasized, however, that these protocols are highly dependent on the fuel cell application, that

is, automotive, stationary, or portable. In this context, we will also focus on the important research on novel catalyst supports, that is, supports that are not based on the typically used high surface area carbons with all their challenges with respect to corrosion but that are made out of alternative materials (e.g, ceramics, metal oxides, and carbides). These more stable supports are only possible thanks to catalyst synthesis routes that are more sophisticated than they ever have been. In the past decade, catalyst synthesis has emerged from an empirical "black art" with only limited control of the final product (the catalyst) into a well-defined "art" in which synthetic chemists can now control almost every aspect of the catalyst nano-particles: particle sizes and their (narrow) distribution[38,39] as well as their shape, that is, their preferential orientation of the surface facets.[40−43] One important aspect, however, is often pushed to the background in the academic environment: namely, the produceability of the catalysts in sufficient quantities and qualities in environmentally friendly processes on an industrial scale.

In this Perspective, a selected summary of electrocatalyst research and development from approximately the past decade will be given. We will focus on fundamental electrocatalyst development as well as on applications of these results in real fuel cell devices. It should be mentioned that we will focus exclusively on electrocatalysis in acidic electrolyte except when specifically noted in the context. Our attempt is to include the most important and promising results achieved in the last 15 years. However, are aware of the fact that our perspective cannot be completely comprehensive, and to a certain point, it reflects our subjective point of view view only, although we tried to include results from many groups in this very lively field of fuel cell R & D.

2. OVERVIEW OF THE IMPROVEMENT IN THE CATALYST ACTIVITY

2.1. Anode Catalyst: Alcohol Oxidation Reaction.
Although in recent years much attention has been paid to the cathode side of low-temperature fuel cells, development of cost-effective direct alcohol fuel cells (DAFC) calls for investigation of low-cost or highly effective electrocatalysts for the oxidation of alcohols at the anode, that is, increasing the current density at low anode overvoltages.

Even if the oxidation kinetics of any alcohol are much slower than for the hydrogen oxidation reaction, the oxidation of alcohols (e.g., methanol and ethanol) is attractive, since these fuels exhibit a high volumetric energy density, and their storage and transport are much easier as compared with hydrogen. For this reason, many scientific efforts are being carried out to develop more efficient and durable anode electrocatalysts for DAFC.

The most common and commercially available is the direct fuel cell driven by methanol oxidation in acidic media. Similar to the cathode side, platinum or platinum-based materials show the best performance toward the oxidation of methanol. The electrochemical oxidation of methanol has been extensively studied over the last 40 years as the result of their importance in the development of methanol fuel cells. It is possible to find in the literature a significant number of studies for methanol oxidation over Pt and Pt alloy surfaces (from well-defined surfaces to supported nanoparticles) that provided insight to establish the mechanistic pathways of the reaction.[30,33,44−55] However, a detailed understanding of the elementary steps in the mechanism is still under debate. In brief, methanol

oxidation follows a dual path mechanism over Pt at sufficiently high potentials involving both "indirect" and "direct" pathways. Unfortunately, the indirect path proceeds via the formation of CO poisoning,[56−58] followed by its subsequent oxidation to CO_2. To get a clear understanding of the mechanism of the oxidation of CO and formic acid oxidation, many different aproaches and techniques have been employed,[28−30,33,59−66] many of them similar to those now employed in the studies of higher alcohols (see below).

In addition to the CO poisoning of the surface, one of the most important drawbacks in the implementation of methanol in fuel cells is methanol's relatively large toxicity. For this reason, higher-molecular-weight alcohols and polyalcohols are under current study as promising fuels due to their low toxicity together with their high specific energy. The most desirable of this group of alcohols are ethanol, ethylene glycol, and glycerol, since they can be obtained from biomass feedstocks.[67−74] However, it is very difficult to have complete mineralization of these alcohols on platinum or platinum alloys, that is, their total oxidation to CO_2.[75−78]

Special attention has been paid to the oxidation of ethanol, which presents a high theoretical energy content of 8 kWh $kg^{−1}$, calculated on the basis of 12 electrons for its total oxidation to CO_2.[79] However, ethanol oxidation on platinum surfaces occurs by different reaction pathways, as is shown in Figure 1. Large
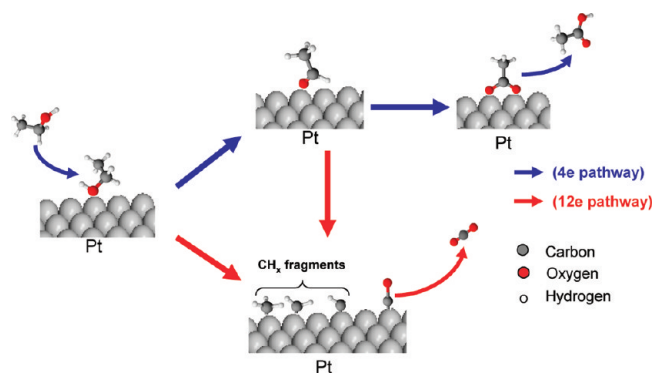

Figure 1. Schematic representation of the reaction mechanism pathways of ethanol electrochemical oxidation on platinum electrodes in acidic media.

amounts of strongly adsorbed intermediate species of partially oxidized products (e.g., CO, CH_x fragments, acetaldehyde, and acetate) are generated in these pathways, diminishing the total efficiency of the system. By using ATR-SEIRAS (attenuated total reflection surface enhanced infrared absorption spectroscopy), Shao and Adzic[80] showed that adsorbed acetate is one of the main reaction products during ethanol oxidation on Pt film electrodes in an acidic electrolyte and remains adsorbed, even at high potentials.

Despite the large efforts dedicated to elucidate the reaction mechanism and the parameters that influence the reaction pathways, there are still significant issues unrevealed. Studies on single-crystal surfaces have led to the determination of surface reaction mechanisms and identification of physical parameters such as electronic and surface atomic structure, respectively. In recent years, Feliu's group[70,81−83] and Koper 's group[68,78,84] have outlined that ethanol oxidation shows a significant degree of surface structure sensitivity, and the reaction mechanism strongly depends on the surface structure of the platinum electrode. Lai et al.[69,84] concluded that the total oxidation

activity increases with the concentration of defect sites (steps). The authors also suggest that the C−C bond-breaking step occurs preferentially in the acetaldehyde molecule.[68,78] On the other hand, Colmati et al.[83] showed that the Pt(110) electrode exhibits the highest catalytic activity for the splitting of the C−C bond, leading to the formation of CO, whereas in a pseudoperfect Pt(111) electrode, the formation of CO is negligible. The main reaction product is acetic acid during the oxidation of ethanol on the pseudoperfect Pt(111) electrode, and acetaldehyde is formed as a secondary product.

Extrapolation of the reaction mechanisms established on model single-crystal surfaces to rational designed nanocatalysts is not straightforward, and the detailed mechanism for the morphology-dependent activity still remains elusive. However, in refs 85−87, an electrochemical method for the synthesis of high−index tetrahexahedral Pt nanocrystals [(100) steps on (100) terraces] is described. These nanocrystals show enhanced catalytic activity per unit surface area in the electrooxidation of formic acid and ethanol (see Figure 2). This behavior was attributed to the high density of stepped atoms on the surfaces of the particles.
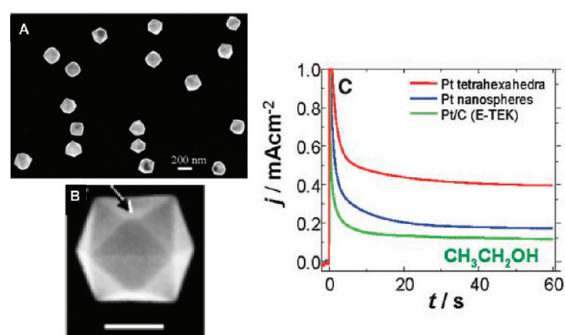

Figure 2. (A) Low-magnification and (B) high-magnification SEM images of high-index tetrahexahedral Pt nanoparticles with growth time of 60 min. (C) Comparison of the transient current density curves of ethanol oxidation at 0.30 V for the of high-index tetrahexahedral Pt nanoparticles, Pt nanospheres, and Pt/C catalyst. Reprinted with permission from ref 87.

In contrast, the Adzic group[88,89] outlined a significant morphology effect on the reaction rates of ethanol oxidation on spherical Pt nanoparticles and ultrathin Pt nanowires. Electrocatalytic tests have demonstrated that the Pt ultrathin nanowires exhibited greatly enhanced activity and efficiency toward ethanol oxidation as a result of a specific ensemble of large crystal facets and a small density of defect sites distinctly different from the commercial Pt spherical-type catalysts. This unique balance between terrace and step sites led to an efficient removal of surface CO_{ads}. The enhancement is reflected by a negative shift in the onset potential of the ethanol oxidation and high current density with at least 2-fold enhanced activity in comparison with the commercial Pt spherical-type catalysts. These results are clearly different from those presented by Na et al.,[87] described above, and therefore highlight the importance of providing new insights of the structural effects in the ethanol oxidation mechanism for the design of novel nanocatalysts.

Outstanding efforts are being carried out to develop new alloy catalysts for DAFC anodes with low platinum loadings and showing a larger efficiency toward the oxidation of alcohols with relatively fast kinetics (comparable to H_2 oxidation) and large durability. Essentially, scientists attempt to develop

catalysts that avoid the poisoning effect of adsorbed intermediate species during ethanol oxidation. A significant enhancement of the electrocatalytic activity of platinum has been reported by modifing or alloying the platinum: PtRu,[76,82,90−94] PtSn,[75,79,81,95,96] PtMo,[97] and PtRh.[93,98]

When Ru is present in the alloy, Ru acts as an oxygen supplier at low potentials, diminishing the poisoning effect from the metastable intermediates,[94] similar to that discussed for the oxidation of methanol.[53] In addition, it is suggested that the presence of Ru in a Pt surface reduces the number of neighboring Pt sites inhibiting the dissociative adsorption of ethanol.[90]

Concerning the catalyst composition−performance relationship of PtRu catalysts, there is no clear agreement in the literature. Spinace et al. reported an improvement in the reactivity of ethanol oxidation for a 30% Ru content catalyst;[99] however, other reports claim optimum activity toward the ethanol oxidation for a 40% Ru content.[90,97] Without going into detail here, similar discussions can be found with respect to the (surface) composition of PtRu catalysts for methanol oxidation, too. The reason for these cross-study discrepancies typically can be found in the uncertainty of the surface compositions of the catalysts used. Especially, careful surface composition−reactivity studies, as performed in the electrocatalysis of methanol oxidation by Gasteiger et al.,[53,55] is missing for ethanol oxidation.

The presence of Sn in a PtSn catalyst favors dissociative adsorption of ethanol. Regarding the optimum Sn bulk composition on the catalyst, Lamy et al.[100] have reported that the most favorable Pt/Sn content ratiois in a wide range (9:1−4:1), whereas Zhou et al.[101] found the optimum Sn content in the range 33−25%. Further studies on the effect of the surface composition on a well-defined alloy single-crystal are required. In terms of the mode of action of Sn in PtSn ethanol oxidation catalysts, strong disagreement exists. Colmati et al.[102] suggest that the high selectivity of this type of catalyst toward the oxidation of ethanol to CO_2 is attributed to the facility to the breaking of the C−C bond at lower potentials. However, results from Wang et al.[103] conclude that the addition of Sn does not enhance the activity for C−C bond breaking. Interestingly, in situ infrared spectroscopy and online differential electrochemical mass spectrometry measurements (see Figure 3) have revealed that the higher ethanol oxidation current density on the Pt_3Sn/C catalyst at potentials below 0.6 V is due to a higher yield of C_2 products and not to an improved complete ethanol oxidation to CO_2.

For this reason, the task of finding a catalyst with the ability of improved complete oxidation of ethanol to CO_2 at lower potentials remains unsolved. Ternary alloys present higher activity than the original mono- and bimetallic counterparts. The addition of a third component usually modifies the electronic and structural characteristics of the alloys, eventually leading to a better catalyst. In recent years, many groups have paid special attention to the performance of ternary alloys with oxophilic atoms, such as PtRuSn,[104] PtRhSn,[105] PtMoIr,[106] PtRuMo,[107,108] or PtSnMo.[109] It is generally accepted that the presence of oxophilic atoms in the surface alloy enhance the oxidation of water, leading to the early formation of adsorbed hydroxides, which can act as an oxidant of the strongly adsorbed intermediate species. For example, the incorporation of different amounts of MoO_x-like species in PtRu systems appears to minimize CO poisoning of the Pt and Ru surfaces vs the PtRu/C catalyst.
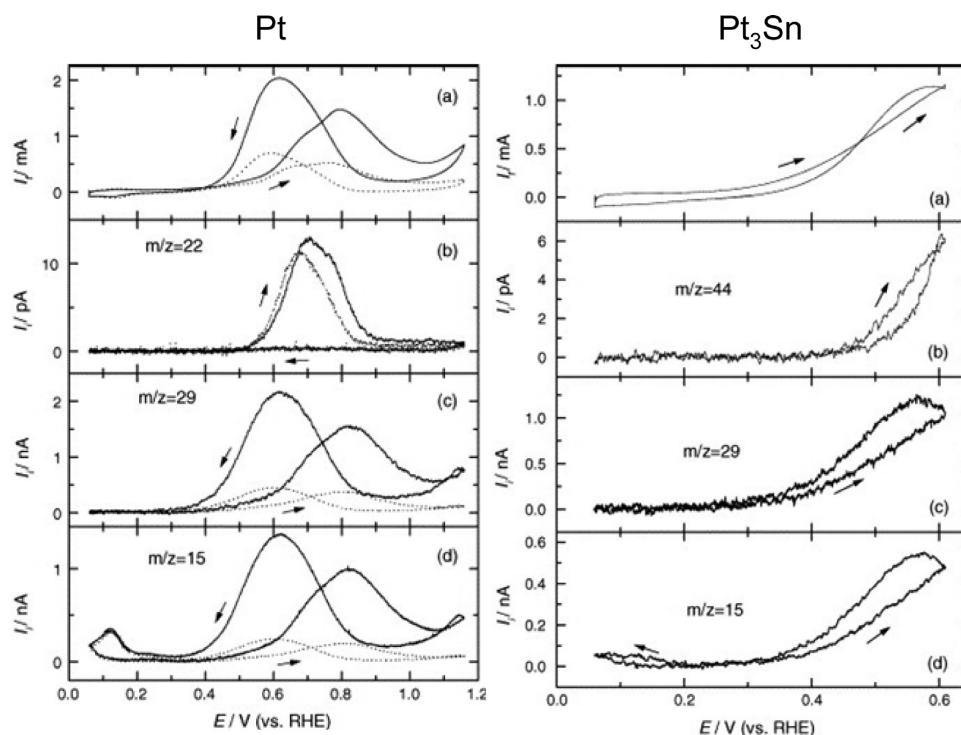
Figure 3. Simultaneously recorded CVs (a) and MSCVs for $m/z = 22$ (double ionized CO_2^+ fragment), $m/z = 44$ (CO_2^+ fragment and CH_3CHO^+), $m/z = 29$ (CHO^+ fragment), $m/z = 15$ (CH_3^+ fragment) for the oxidation of ethanol on a Pt/Vulcan and Pt$_3$Sn catalyst (as indicated in the Figure) in 0.1 M ethanol + 0.5 M H_2SO_4 (—) and in 0.01 M ethanol + 0.5 M H_2SO_4 (······) solution (scan rate: 10 mV s^{-1}). Arrows indicate the direction of potential scan. 0.1 M ethanol + 0.5 M H_2SO_4 solution. Reprinted with permission from ref 103.

Regarding these ternary alloy catalysts, it was found that the higher ethanol oxidation current density on the PtRuMo/C catalyst with the higher amount of Mo results from higher yields of C_2 products and not from an improved complete ethanol oxidation to CO_2.[107] On the other hand, Kowal et al.[110] have shown that the PtRhSnO$_2$/C electrocatalyst is capable of effectively splitting the C–C bond in ethanol at room temperature in acid solutions, facilitating its oxidation at low potentials to CO_2 with high efficiency. The reported catalytic activity of the PtRhSnO$_2$/C electrocatalyst is ~100 times higher than the corresponding activity of Pt/C. The authors suggest that the catalytic activity of the PtRhSnO$_2$ alloy is due to the synergy between the three constituents of the electrocatalyst. It is also proposed by the authors that the dissociation of the water occurs on the SnO$_2$, providing OH species that oxidize the intermediate CO at Rh sites while the Pt atom facilitates the ethanol dehydrogenation.[110]

2.2. Cathode Catalyst: Oxygen Reduction Reaction. The oxygen reduction reaction is probably one of the most extensively studied electrocatalytic reactions and is still the most serious challenge for the commercialization of PEFCs. Platinum is the best base metal for the catalysis of the ORR, but due to sluggish reaction kinetics that includes a multielectron process with a number of elementary steps involving different reaction intermediates, the ORR requires high overpotentials (0.3–0.4 V). To overcome this main electrochemical voltage loss in PEFCs, the catalysis of the ORR requires high loadings of platinum in fuel cell cathodes, typically in the range of 0.1– 0.5 mg/cm^2.

A simplified reaction scheme with only two products, H_2O_2 and H_2O, can be depicted from Figure 4.[56,111] Ideally, O_2 reduction is a four-electron transfer process from O_2 to H_2O in both acid and alkaline aqueous electrolytes.[10,112] However, the
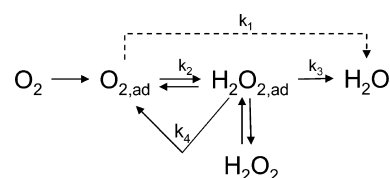

Figure 4. The oxygen reduction reaction mechanism on Pt.[56,111]

exact mechanism remains unknown. Although some authors proposed the dissociative mechanism, others defend the associative mechanism. In both cases, the intermediate formation and the reactive species are still under discussion.[10] Although the experimental prove is still missing, there are strong experimental hints that the ORR proceeds via peroxo species; that is, the first electron transfer occurs to the adsorbed oxygen molecule. For instance, on Pt and many other noble metals, RRDE measurements always show that peroxide detection during the ORR always follows the activity of the catalyst toward the reduction of H_2O_2 (for a discussion, see e.g. refs 56, 111, 113, 114) In addition, chemical intuition would favor a molecular rather than a dissociative adsorption of oxygen on a Pt surface highly covered by relatively strong adorbates (e.g., water, adsorbed hydroxy species, anions, H$_{UPD}$; in contrast to O_2 adsorption in UHV, where the molecule is dissociating) which makes a serial reaction pathway more likely.

Although across the past three decades, many authors have been discussing about the surface structure dependence of Pt toward the ORR under different conditions, it was not until the end of the 1990s when Markovic, Ross, and co-workers reported trends of the low-index planes in perchloric[114] and sulfuric acid[113] as well as alkaline[115,116] solutions. Markovic et al. found that the activity for ORR in 0.1 M HClO$_4$ decreases in
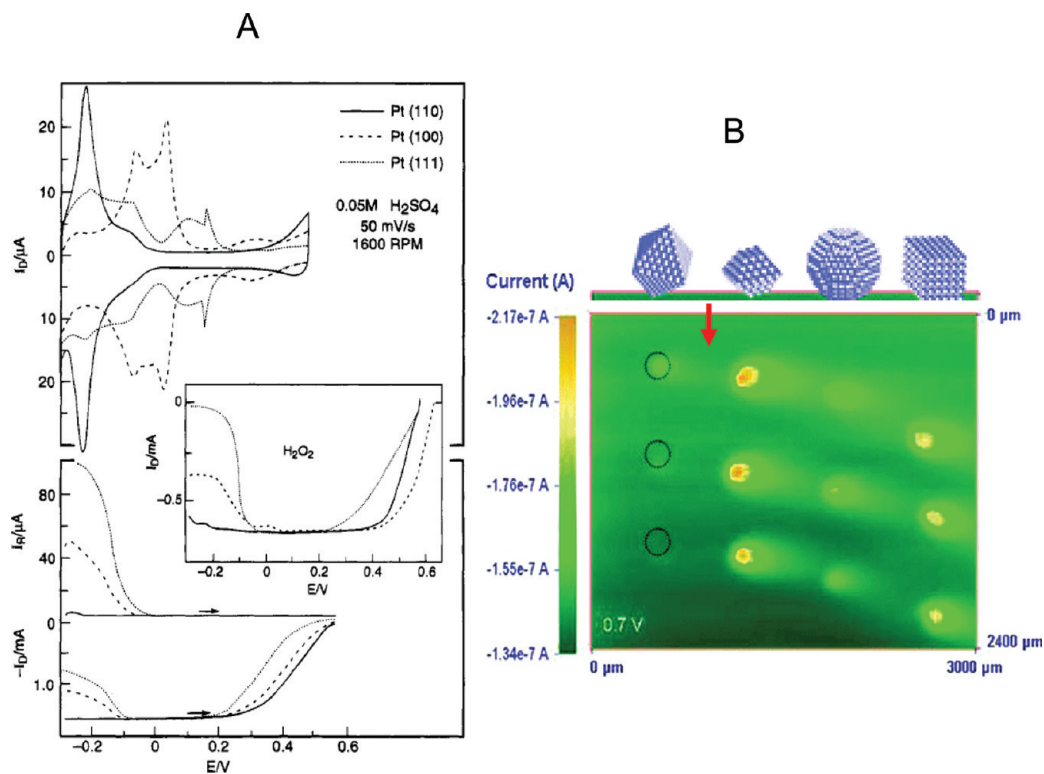
Figure 5. (A) Top: cyclic voltammetry of Pt(*hkl*) in oxygen-free electrolyte in the RRDE assembly (fifth sweep). Bottom: disk (I_D) and ring (I_R) currents during ORR on Pt(*hkl*) (ring potential = 0.95 V). Inset: reduction of $1.2 \times$ M H_2O_2 on Pt(*hkl*) mounted in the RRDE assembly (0.05 M H_2SO_4, 50 mV/s, 1600 rpm). Reprinted with permission from ref 113. (B) Scanning electrochemical microscopy TG/SC (tip generation/substrate collection) image displaying the reduction current collected for ORR in 0.5 M H_2SO_4 solution at a Pt nanoparticles array. This array presents three equal rows composed of spots of four different types of shape-controlled Pt nanoparticles, and its potential is held constant at 0.7 V. Scan rate = 125 μm/s. Reprinted with permission from ref 118.

the sequence (110) > (111) > (100), whereas the reactivity in H_2SO_4 increased in the sequence (111) < (100) < (110) (Figure 5A).[113] These differences in the sequence are ascribed to the strong (bi)sulfate anion adsorption on the highly coordinated surfaces. Therefore, it is important to consider the strength of the anion adsorption and its surface-structure-dependent adsorption properties to understand the oxygen reduction reaction. These findings acknowledged the importance of spectator species on reaction rates and the important influence of the pre-exponential $(1 - \Theta_{spectator})$ term in the electrochemical kinetic rate expression.[111]

In addition to the studies on the basal planes, Kuzume et al.[117] have contributed by understanding the effect of step density and geometry on the ORR. The authors demonstrate that the low catalytic activity of the Pt(111) electrode with respect to the stepped-surface electrodes in sulfuric acid media is related to the specific adsorption and the bidimensionally ordered adlayer of (bi)sulfate on Pt(111). As the (bi)sulfate/platinum surface interaction decreased for relatively narrow terraces, small differences in the catalytic activity for the stepped surfaces were found.[117]

Very recently, surface structure dependence studies on (*hkl*) electrodes have been extended to studies on well-defined nanoparticles. For instance, by using scanning electrochemical microscopy, Sanchez–Sanchez et al.[118] showed improved catalytic activity for the ORR on hexagonal Pt nanoparticles in $HClO_4$ and H_2SO_4 (Figure 5B). In addition, this study also outlined that preferentially oriented Pt NPs significantly change their catalytic activity because of the specific adsorption of

(bi)sulfate anions, confirming the earlier results on single-crystal electrodes.

Even though well-known from the PAFC related catalyst development in the 1970s and 1980s,[119,120] some authors report the enhancement in the ORR by alloying of the Pt catalyst with Ni, Cr, and Co. It was not until the work of Mukerjee et al.[121] and Toda et al.[122−124] when Pt alloy catalysts were considered a good candidate toward the ORR in a low-temperature PEFC environment. Toda et al.[122−124] reported the maximum activity toward the ORR for Pt alloys with a 30, 40, and 50% content of Ni, Co, and Fe, respectively, which presented 10, 15, and 20 times larger kinetic current densities than pure Pt (as discussed previously, however, in these studies, the activity of pure Pt is ~10× lower compared with other studies; for a discussion, please refer to ref 125).

The catalytic activity of Pt toward the ORR strongly depends on the adsorption energy and dissociation energy of O_2 and also on the adsorption energy of the OH species on the surface.[126,127] These parameters are strongly affected by the Pt−Pt interatomic distance[126,127] and also by the Pt d-band vacancy. The authors suggest that by the addition of the second metal into the Pt lattice (up to 30−50 atom %), the 5d vacancies of the surface increase (Ni, Co, or Fe has more 5d vacancies than Pt). Such an increase of 5d vacancies led to an increased 2p electron donation from O_2 to the Pt, resulting in an increased θ_{O_2} and a weakening of the O−O bond. However, the addition of larger amounts of the second metal beyond the optimum content results in an increase in the 5d vacancy of the electrode; thus, the Pt−O bonding becomes stronger, and the
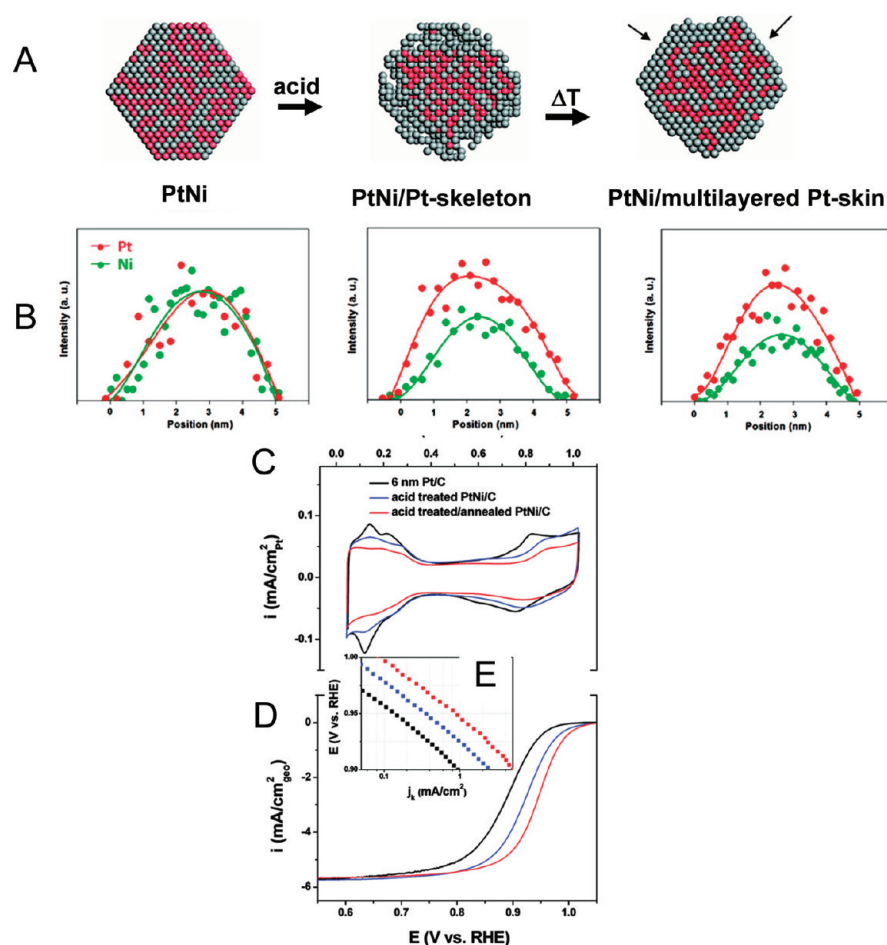
Figure 6. (A) Cross section views of the nanostructures depicted by atomistic particle simulation. (B) Composition line profiles (normalized for Pt–L peaks) obtained by energy-dispersive X-ray spectroscopy with an electron beam (~2 Å in spot size) scanning across individual catalyst particles The figure is also organized in columns for the as-prepared (left), acid treated (middle), and acid treated/annealed (right) PtNi/C catalysts, respectively. (C) Cyclic voltammograms, (D) polarization curves, and (E) Tafel plots with the specific activity (j_k, kinetic current density) as a function of electrode potential, in comparison with the commercial Pt/C catalyst. Estimation of electrochemical surface area was based on integrated H_{upd} for the Pt/C and acid treated PtNi/C catalysts and CO_{ad} stripping polarization curvefor the acid treated/annealed PtNi/C catalyst. Reprinted with permission from ref 135.

back-donation turns out to be difficult, resulting in a lowered ORR rate.

Since the work of Toda, many studies have been carried out concerning the catalytic activity of supported Pt-alloy nanoparticles toward the oxygen reduction reaction.[13,38,128−133] Yang et al. found that the PtNi bimetallic catalysts with different Pt:Ni atomic ratios exhibited an enhancement factor of ~1.5−3 in the mass activity and of ~1.5−4 in the specific activity for the ORR in $HClO_4$. The authors reported that the maximum activity of the Pt-based catalysts is reached for catalyst with a Ni content of 30−40 at. %.[130] Similarly, Paulus et al. reported a small mass activity enhancement of ~1.5 for the 25% Ni and Co catalysts and a more significant enhancement of a factor of 4 for the 50% Co.[131,133] In the study by Huang et al., PtCo alloy nanoparticles exhibit a mass activity enhancement of a factor of ~1.3−3.2 and of a factor of ~1.2−2.2 in the specific activity for the ORR when compared with Pt toward the oxygen reduction reaction.[132] In addition to the effect of the concentration of the second metal on the alloy, others studies were performed to determine the size-dependent activity for the oxygen reduction reaction. It was found, for example, that the ORR activity of Pt_3Co decreases with the

particle size. The optimal size for maximal mass activity in Pt_3Co nanocatalysts was estimated to be around 4.5 nm.[132]

Unfortunately, several variable parameters, such as the already mentioned particle size, shape, and composition of the Pt alloy-supported catalyst can affect the results, making difficult the correct analysis and comparison in terms of specific activities, especially when the values are normalized by Pt surface area and not per mass of catalyst. In this sense, several studies were carried out on bulk alloy and single-crystal electrodes, and theoretical calculations have given clear insight into the effect of the second metal in the alloy catalyst. In all the cases, it was found to be important to control the relation between the surface and the bulk composition of the alloys. PtNi and PtCo alloys can exhibit highly structured compositional oscillations in the first three atomic layers.[134] By different methodologies, it is possible to modify and control the composition of these top layers, leading to the so-called "skeleton−skin" or "core−shell" structure, with Pt depletion in the top layers (Figure 6A and B).

Stamenkovic et al.[136,137] employed UHV and in situ electrochemical methods to prepare, characterize, and study the oxygen reduction reaction on polycrystalline Pt_3Ni and Pt_3Co bulk alloys in acid electrolytes. In these studies,
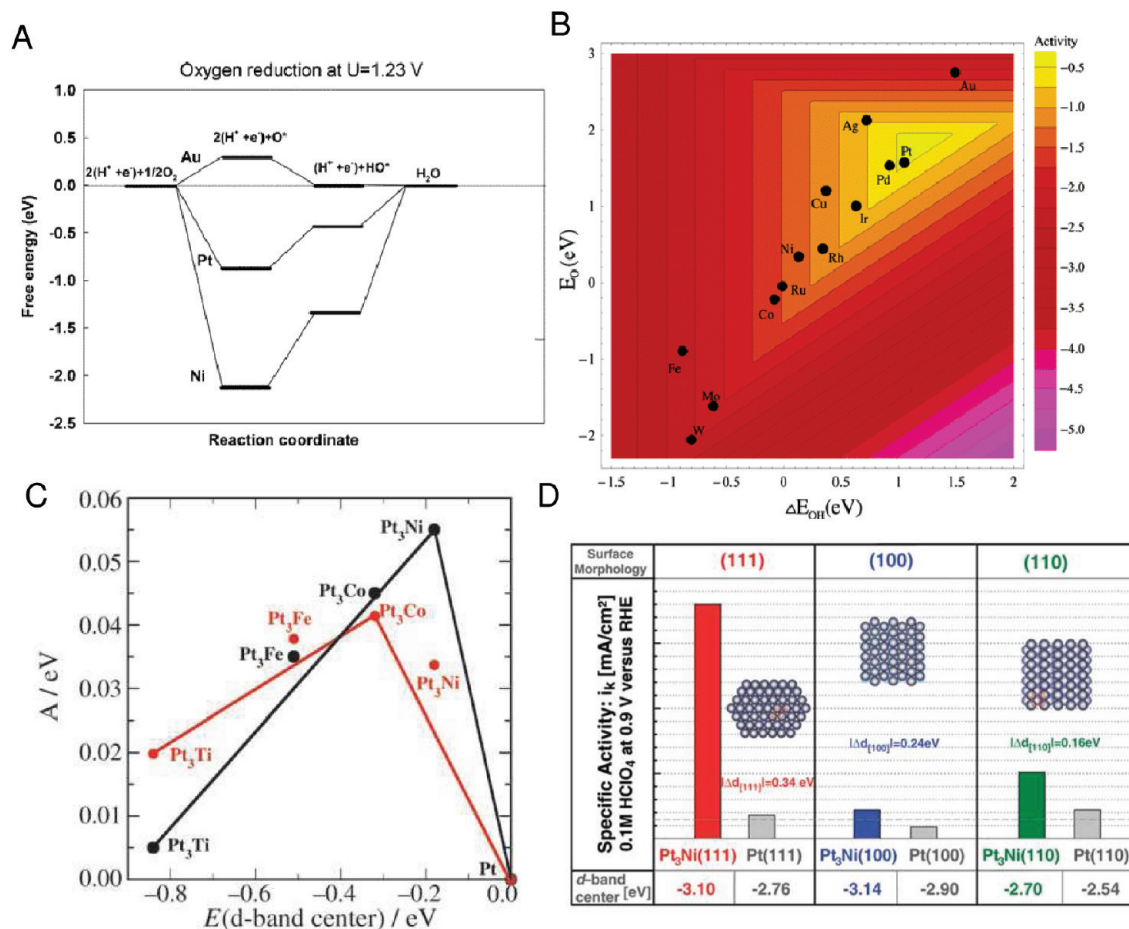
Figure 7. (A) Free-energy diagram for oxygen reduction at the equilibrium potential $U_0 = 1.23$ V over Pt, Au, and Ni. (B) Trends in oxygen reduction activity plotted as a function of both the O and the OH binding energies. Reprinted with permission from ref 10. (C) Activity versus the experimentally measured d-band center relative to platinum. The activity predicted from DFT simulations is shown in black, and the measured activity is shown in red. Reprinted with permission from ref 138. (D) Influence of the surface morphology and electronic surface properties on the kinetics of ORR. RRDE measurements for ORR in $HClO_4$ (0.1 M) at 333 K with 1600 rpm on $Pt_3Ni(hkl)$ surfaces as compared with the corresponding Pt(hkl) surfaces (a horizontal dashed gray line marks specific activity of polycrystalline Pt) are shown. Specific activity is given as a kinetic current density ik, measured at 0.9 V versus RHE. Values of the d-band center position obtained from synchrotron-based, high-resolution ultraviolet photoemission spectra are listed for each surface morphology and compared between corresponding $Pt_3Ni(hkl)$ and Pt(hkl) surfaces. Reprinted with permission from ref 23.

polycrystalline bulk alloys of Pt_3Ni and Pt_3Co were prepared to have two different surface compositions: one with 75% Pt (i.e., bulk compositions) and the other with 100% Pt (so-called "Pt-skin" structure). It was found that in 0.5 M H_2SO_4, the activity increased in the order $Pt_3Ni > Pt_3Co > Pt$; whereas in 0.1 M $HClO_4$, the catalytic enhancement was greater than in sulfuric acid for all the catalysts, and the order of activities was "Pt-skin" > $Pt_3Co > Pt_3Ni > Pt$. The maximum catalytic activity was found on the "Pt-skin"–Pt_3Co in 0.1 M $HClO_4$: 3–4 times higher than for pure Pt.

Kinetic analyses revealed that kinetic parameters for the ORR and the production of H_2O_2 on the Pt_3Ni, Pt_3Co, and "Pt-skin" alloys are the same as on pure Pt, which implies that the reaction mechanism is the same as on pure Pt. The enhancement factor induced by the alloying component or the formation of a Pt-skin was interpreted by the reduced adsorption of oxygenated species from water, that is, a ~20–30 mV shift of the formation potential of OH_{ad} to more positive potentials on the alloy surfaces, leaving more active Pt sites for the ORR. Stamenkovic et al. found that the relationship between the specific activity and the d-band center position ((1

$- \Theta_{ad}$) and ΔG_{ad}) on the Pt-skin surfaces exhibits a volcano shape (Figure 7C).[138] The reason for that is that the d-band center position controls both this term and the specific activity. These results also predict the higher catalytic activity of Pt_3Ni electrodes.[23] However, as can be seen, the experimental maximum catalytic activity was obtained for Pt_3Co.[138,139] It also has been shown that the different low-index surfaces have markedly different activities toward the ORR in $HClO_4$ solutions following the trend $Pt_3Ni(100)$-skin < $Pt_3Ni(110)$-skin ≪ $Pt_3Ni(111)$-skin (Figure 7D). It is concluded in this report that the oxygen reduction reaction was enhanced by a factor of 10 on $Pt_3Ni(111)$-skin in comparison with the Pt(111).[23] On the basis of our knowledge, this is the best catalytic activity toward the ORR reported in the literature.

In addition to the experimental data on the Pt_3M catalyst, theoretical studies demonstrated that Pt-skin in Pt_3M is a unique surface with special electronic and catalytic properties. The most relevant finding is the fact that the Sabatier model can be used to predict ORR activity. The experimental and theoretical agreement of the simple Sabatier model for the ORR on Pt_3Ni is evident in Figure 7B and C.[140,141]

On the basis of the calculations in ref 12, it was found that the higher activity for Pt$_3$Ni(111) is a result of a better compromise in bond strength to the OOH and OH intermediates species. As can be seen in Figure 7A, the ORR on Pt is rate-limited by the strongly adsorbed OH. On the other hand, the same figure shows that O and OH binds so strongly to the Ni surface that the proton-transfer steps become strongly activated.[10] This is not true of Pt$_3$Ni(111), which instead is limited by the OOH formation step. As previously described by Stamenkovic et al., this volcano curve is ruled by the equilibrium between adsorption energies of intermediates and surface coverage by spectator (blocking) species, and the maximum of the volcano curve defines the maximum catalytic activity.[138,139] In the case of single metals, the maximum activity was found for the Pt catalyst (Figure 7B).

Very recently, these "skin structure" studies have been extended to nanoparticles and inclusive nanoparticles with a well-defined surface structure. Wang et al.[135] developed skin-PtNi nanostructures showing enhanced catalytic activity and also improved catalyst durability for the ORR. The authors showed that in a RDE configuration and after 4000 potential cycles between 0.6 and 1.1 V (0.1 M HClO$_4$, 60 °C), the skin-PtNi/C catalyst had only 15% loss in specific activity, in contrast to 38% for Pt/C. This effect is attributed to the fact that the Pt-skin shields the Ni inside the catalyst and enabled the sustained high catalytic activity. On the other hand, Zhang et al.[142] reported a new synthesis approach of Pt$_3$Ni nanoparticles with (111) and (100) facets. It is shown that the ORR activity on the Pt$_3$Ni with (111) facets is 5-fold higher than the Pt$_3$Ni alloys of a similar size and (100) orientation. In addition, it is also shown that the ORR specific and mass activities of Pt$_3$Ni nanoparticles with (111) facets are 7 and 4 times higher, respectively, than those of the commercial Pt/C catalysts.

Several new catalyst systems have been tested for the ORR since then, for example, multimetallic alloys. One example is Au/FePt$_3$/C prepared by epitaxial growth of PtFe alloy over Au seeds. This system shows an activity enhancement factor of over 7 in specific activity and more than 1 order of magnitude in mass activity in comparison with Pt/C, even after extensive potential cycling.[143] It was observed that the multimetallic Au/FePt$_3$ nanoparticles are not affected by the well-known Ostwald ripening phenomena, in contrast to Pt/C and PtFe/C nanoparticles. On the other hand, the catalytic activity of Au/FePt$_3$/C toward the ORR was similar to that for FePt$_3$/C, which suggests that the Au core does not affect electronic/adsorption/catalytic properties of the surface Pt atoms.

Another approach reported in recent years regarding the improvement in the catalytic activity of the ORR is the dealloying concept proposed by Strasser's group.[144−148] Structural and compositional analysis showed that the resulting dealloyed catalyst consists of a core−shell structure with a Pt-rich shell and a Pt-poor alloy particle core (basically forming a Pt-skeleton type surface with purposely formed extended skeleton shell) . The authors report significant activity enhancements for the ORR after Cu or Co dealloying from PtCu/C, PtCo/C, and PtNi/C alloy nanoparticle electrocatalysts, respectively. After removal of the second metal atoms from the surface region, the resulting particle catalysts showed improvements of 3–6-fold activity over Pt/C catalyst.[146,148−151] The activity enhancement in this type of catalyst is attributed to geometric and strain effects. It is suggested that the surface dealloying creates favorable Pt reactive sites for the ORR. In

addition to the better ORR kinetics, these systems also show improved durability, which will be discussed in section 3.1.

Other alternatives have been proposed to be used as catalyst for the ORR. This is the case of the Au clusters on Pt nanoparticles. Zhang et al. showed that Au cluster stabilize Pt nanoparticles under highly oxidizing conditions by suppressing the Pt oxidation/dissolution during potential cycling without decreasing the oxygen reduction kinetics.[152] PdPt nano-dendrites have been also tested toward the ORR, and they present an improvement of the specific activity by a factor of around 3 vs Pt/C catalysts and around 2 vs Pt black. In this case, the enhancement in activity toward the ORR was attributed to the presence of preferentially exposed (111) facets with some (110) and (311) facets.[153]

In addition to the well-defined nanoparticles and the bimetallic and multimetallic catalyst, a new trend in catalyst designs has been proposed. This trend is based in the modification of the metal surface by nonmetallic molecules that can influence the electronic properties of the metal[154−156] or block the adsorption of poisoning species.[157−159] In particular and regarding the ORR in acidic media, Escudero-Escribano et al. and Strmcnik et al.[157,158] demonstrated that cyanide adsorbates on platinum surfaces can efficiently block the sites for adsorption of spectator oxo anions while providing a sufficient number of free metal sites to chemisorb the O$_2$ molecule and break the O−O bond. In this case, the effect is entirely geometric because the adsorbed cyanide does not influence Pt−O$_2$ or Pt intermediates energetics. The authors show that depending on the anions and cations present in the supporting electrolyte, on the same CN-covered Pt(111) surface, the ORR activities can range from a 25-fold increase to a 50-fold decrease.[157,158]

Although many advances in the ORR have been accomplished in the last years, improvements exclusively due to alloy structure and composition are not sufficient to improve the mass activity and to suit the commercialization requirements of low-temperature fuel cells (see section 1). Snyder et al.[160] adopt another strategy in which tailoring geometric and chemical materials architecture further improve ORR electrocatalysis. The authors show that when a nanoporous composite of PtNi alloy is impregnated with a hydrophobic protic ionic liquid secondary phase with high oxygen solubility, the catalyst presents an extremely high mass activity toward the ORR. In this two-phase confined structure, the oxygen diffusing into the pores would be chemically restricted to remain close by the catalyst surface, even if neither phase were fully saturated. This space limitation increases the frequency of interaction with the catalytic surface and, hence, the overall activity of the ORR. The results presented by the authors demonstrate a high catalytic activity toward the ORR, and they suggest that this kind of strategy could yield mass activities nearly an order of magnitude higher than that of commercial Pt/C.

In this section, we have summarized many new and promising results from the international quest for novel highly active ORR electrocatalysts. However, many of these exciting approaches have been tested and characterized only outside of a PEFC thus far under conditions that are relevant to PEFC operation. Bringing these catalysts into a gas-diffusion electrode or a catalyst-coated membrane and finally into a MEA for fuel cell operation imposes new challenges to transport suitable catalyst properties into real devices without losses of their exciting properties.

3. STABILITY ISSUES

Operation conditions such as temperature, voltage, current, gas partial pressure, relative humidity (RH), or impurities can affect the long-term performance of PEFCs significantly. Therefore, to reach lifetimes of PEFCs as outlined in Table 1, the catalysts and the catalyst layers inside a MEA need to be stable enough to maintain sustained catalytic activities over the PEFC life. Although the mechanisms of degradation are not all fully understood, here, we provide some of the most recent results in the study of the degradation mechanism of the catalyst and the supports.

3.1. Degradation of the Catalyst Active Layer. This part will focus on durability aspects of mainly PEFCs for both automotive and stationary applications. As discussed elsewhere,[161] from a scientific and technical perspective, we need to consider the following question: How can the performance (see section 2.1) and the lifetime of a PEFC be improved with (preferentially) reduced noble metal loading? One of the driving forces is satisfying the technical and scientific goal to design "better" materials, for example, more efficient and stable catalysts, chemically and physically more stable polymers and membranes, or to design "better" interaction of the catalysts and the membrane (e.g., lamination properties, sealing integration).

From a commercial point of view, the necessary lifetime of the fuel cell system is required to make it useful with respect to competing technologies, which in turn can be translated to the simple correlation of longer lifetime that is equivalent to a lower cost (or shorter pay back periods). The underlying challenge for basically all PEFC and component developers is improving durability. The importance of fuel cell durability is clearly recognized, and much of the current research and development is related to this topic (see, e.g., refs 162−165 and references therein).

In what follows, the focus will be on the most important recent results on catalyst and electrode durability used for PEFCs. It should be noted here that in our opinion, electrocatalysis research is not only the study of catalysts with respect to understanding and improvement of actual reaction rates (as described in detail in the previous sections), an at least equivalently important task is the understanding of catalyst durability in the technical environment. The term technical environment also includes the knowledge of the conditions an electrocatalyst inside a technical electrode will fail. Therefore, understanding the predominant degradation mechanisms is crucial to understanding the electrocatalyst (defined as the active phase and the support) properties during operation. In the context of this section, we therefore purposely refer to the topic of catalyst durability also from the technical perspective of fuel cell operating conditions.

The two predominant processes affecting catalyst lifetime in an operating PEFC are the corrosion of the carbon supports and the loss of active Pt surface area during operation. Especially, improvement of the cathode catalyst is of great importance, to reach the performance and durability requirements for both automotive and stationary PEFC applications (see Table 1). The typically used cathode catalyst consists of Pt or Pt-alloy (with, e.g., a typical base metal such as Ni or Co as the alloying component) nanoparticles supported on high-surface-area carbon supports. Although carbon supports are known to be thermodynamically unstable at electrochemical potentials above 0.206 V_{NHE},[166] it still represents the catalyst

support of choice for PEFC electrocatalysts for the following reasons: (i) high electronic conductivity in the range of approximately >1 S cm^{-1}; (ii) high specific surface area[166] of ~50−800 m^2/g$_{carbon}$; (iii) the ability to form highly porous structures with pore sizes of 20−100 nm when manufactured in a gas diffusion catalyst layer;[167] and (iv) the very sluggish kinetics of the carbon oxidation reaction (COR), eq 1 at potentials below 0.80 V,[168] therefore enabling relatively stable fuel cell operation under regular load conditions.

$$C + 2H_2O \rightarrow CO_2 + 4H^+ + 4e^- \qquad E_0 = 0.206V_{NHE} \tag{1}$$
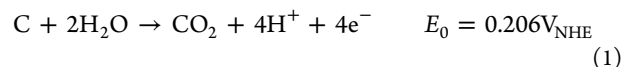
In a laboratory environment, the upper potential limit of the cathode can typically be controlled in an appropriate way. In an operating fuel cell system, however, electrochemical potentials can, indeed, exceed 0.8 V due to specific operating conditions. In automotive fuel cell applications, for instance, analysis of different driving cycles leads to the assumption that during the fuel cell system's life (5000 h; see Table 1) ~300 000 cycles between 0.7 and 0.9 V (or open circuit potential) will be performed.[169] In addition, cathodic potential excursions to values up to 1.5 V have been measured during start/stop cycles.[170−172] The predominant mechanism during start/stop cycling affecting cathode durability is corrosion of the cathode due to potential excursions to these high potentials.[170] Cathode carbon corrosion during start/stop cycling occurs when the cathode electrolyte potential excurses to high values when H$_2$/air (Air/H$_2$) fronts are passing through the anode while the cathode compartment is filled with air (see Figure 1, this scenario occurs through oxygen diffusion processes into the anode compartment, which cannot be avoided in practice). The anode potential is defined by the hydrogen potential, which causes the oxygen in the anode to be instantaneously reduced to water. During the ORR at the anode side, the used protons need to be generated in an oxidation reaction at the opposite side at the cathode, which is either carbon oxidation (eq 1) or oxygen evolution (eq 2), both being faradaic reactions. In parallel, oxidation of Pt can take place at these potentials, as well (eqs 3 and 4; Figure 8, right-hand side; pseudocapacitive reactions).
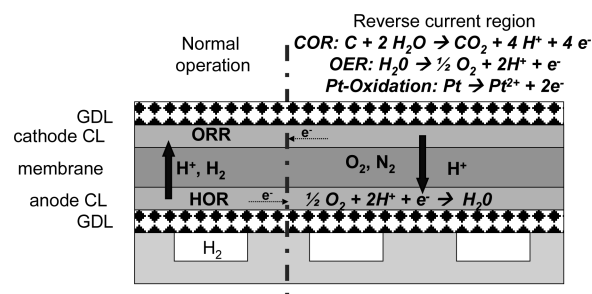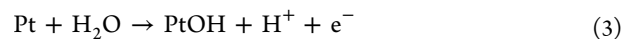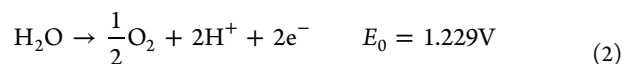
$$H_2O \rightarrow \frac{1}{2}O_2 + 2H^+ + 2e^- \qquad E_0 = 1.229V \tag{2}$$

$$Pt + H_2O \rightarrow PtOH + H^+ + e^- \tag{3}$$

$$PtOH \rightarrow PtO + H^+ + e^- \tag{4}$$

Figure 8. Start/stop induced cathode carbon corrosion mechanism and the reverse-current region. Figure and description of the effect are taken from ref 172.

The equilibrium potentials of reactions 3 and 4 have been estimated to be 0.85 and 1.0 ± 0.05 V vs RHE.[173] In parallel to the proton forming reactions, 1−4, Pt can be dissolved according to eq 5

$$Pt \rightarrow Pt^{2+} + 2e^- \qquad (5)$$

By examination of the respective Pourbaix diagram,[174,175] reaction 5 is expected to occur in a triangular region under the present pH conditions between approximately 0.90 and 1.25 V.

Under the described conditions (Figure 8), reactions 1 through 5 can take place opposite the ORR at the anode side. This is called the reverse current region.[170] Simultaneously, in the normal operation region (Figure 8, left-hand side), hydrogen and oxygen are oxidized and reduced, respectively, as usual. Both regions are electrically connected through the electrode and gas diffusion layer materials. Basically, the fuel cell is internally short-circuited. One can consider the normal operation region as a power source and the reverse current region as a power sink. Locally around the H_2/air (Air/H_2) front, the potential of the cathode can be between 1.3[172] and 1.5 V.[170] Because of these high potentials, severe oxidation of the cathode can take place if no precautions are taken, which not only leads to loss of carbon surface area and detachment of Pt-nanoparticles, but also can result in complete deterioration of the catalyst layer and even loss of the electrode integrity with rapid failure of the fuel cell.[168,176]

Similar severe carbon corrosion effects on the cathode can be observed during local anode hydrogen starvation.[177] The most deleterious and fast carbon corrosion in a fuel cell combined with rapid cell failure will occur during gross anode starvation (e.g., under conditions of high fuel utilization operation), which will instantaneously lead to reverse cell polarization and corrosive loss of the anode carbon materials in the fuel cell.[178]

As an example of the deleterious effects of start/stop cycling on the performance of a fuel cell, we refer to Figure 9. It is
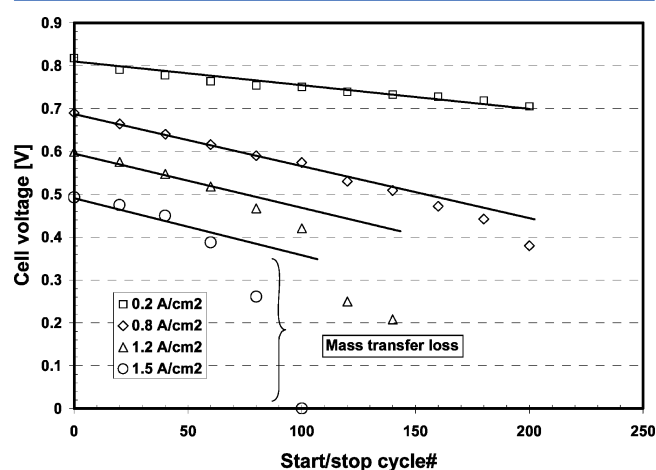

Figure 9. Start/stop induced voltage losses in an operating fuel cell using a commercial carbon-supported cathode catalyst. (80 °C, 66% RH$_{inlet}$, residence time H_2/Air front 1.3 s). Reprinted with permission from ref 168.

shown that the fuel cell voltage already decreases after a few tens of start/stop cycles (e.g., ca. 100 mV voltage loss after ca. 70 cycles; see Figure 9 at realistic cell voltages between 0.6 and 0.7 V initial potential) if no precautions are taken.

Close inspection of these data reveal that especially at high current densities, the performance losses are drastic, which

points to a significant increase in the mass transport overpotentials (quantified, e.g., in a recent publication by Hartnig and Schmidt[179]) and which directly points to changes in the catalyst layer morphology due to the corrosion of the carbon. This morphology change recently was visualized by Schulenburg et al.[180] using a 3D-rendering of SEM pictures from catalyst layer slices prepared by a focused ion beam (FIB). Figure 10 visualizes the porous structure of a cathode catalyst layer (Gore Primea 5710) before and after 1000 start−stop cycles. Initially, the pores in the catalyst layer are well interconnected with an overall porosity of ∼40%, whereas after start−stop cycling, the porous layer is basically collapsed with isolated pores and an overall porosity of only ∼5% combined with a reduction of the accessible Pt surface by 85%.[180] Qualitatively similar results have been found by 3D electron tomography in the study by Liu et al.[35] in catalyst layers after local fuel starving.

To overcome this critical stability issue of the cathode catalyst, specifically under start/stop operating conditions or potential cycling, in addition to engineering solutions,[178] several possibilities on the materials level are discussed in the literature:

(i) Implementing a highly active oxygen evolution catalyst in the fuel cell cathode to favor oxygen evolution over carbon corrosion during the passing of the H_2/air (air/H_2) front.[181,182] The shortcoming of this approach is typically found in the difficulty in forming reliable porous catalyst layers in the mixed carbon supported reduction and the typical evolution catalyst with proper mass transport properties (with the formation of the aforementioned pores sizes between 20 and 100 nm) and the additional cost of highly active oxygen evolution catalyst (e.g., Ir or Ru oxide-based systems).

(ii) Using a highly selective anode electrocatalyst, that is only able to oxidize hydrogen, but not to reduce oxygen, which would avoid the internal shorting of the cell. Some basic research is carried out on this topic[183] in which Pt single crystal electrodes have been modified by a self-assembled monolayer of calix[4]arene showing almost 100% selectivity toward hydrogen oxidation, even at potentials close to the reversible hydrogen potential. However, until now, to the best of our knowledge, no data from a durable catalyst which have been implemented into a operating fuel cell is yet published.

(iii) Exchanging typical high surface area carbon black supports in the cathode catalyst with highly graphitized carbon blacks. This is the most widely used approach, which was also shown to improve the durability of the fuel cell cathodes under operating conditions (see, e.g., refs 161, 167, 168, 179, 184). However, due to the typical significant reduction of the carbon surface upon graphitization, catalyst dispersion can be significantly reduced. In addition, a porous structure formation with the required pore size distribution becomes critical in this case, as well. It should be mentioned that graphitized carbon can be oxidized under these conditions too, so the corrosion issue is not avoided, just kinetically delayed.[168]

(iv) The most straightforward approach would be the exchange of carbon as support material in the cathode catalyst, thereby avoiding corrosion completely. Several approaches using metal oxides and other metal-based
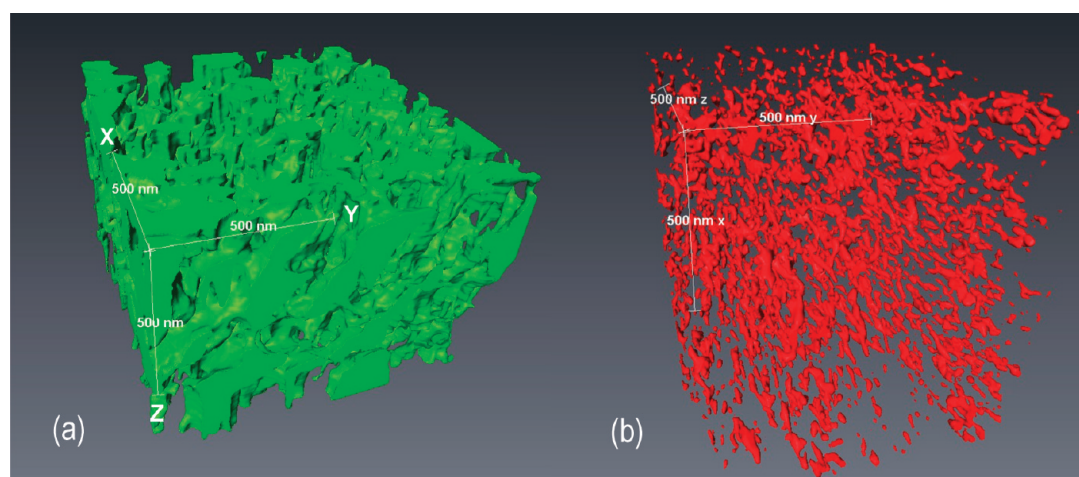
Figure 10. Three-dimensional pore structure of the pristine cathode catalyst layer (a) and after start/stop cycling (b). The colored phase represents the pore structure. 1000 simulated start−stop cylces (60 s alternating H_2 and air purging of the anode), 16 cm^2 single cell, 80 °C, 70% RH, parallel load of 3 mΩ cm^2. Reprinted with permission from ref 180.
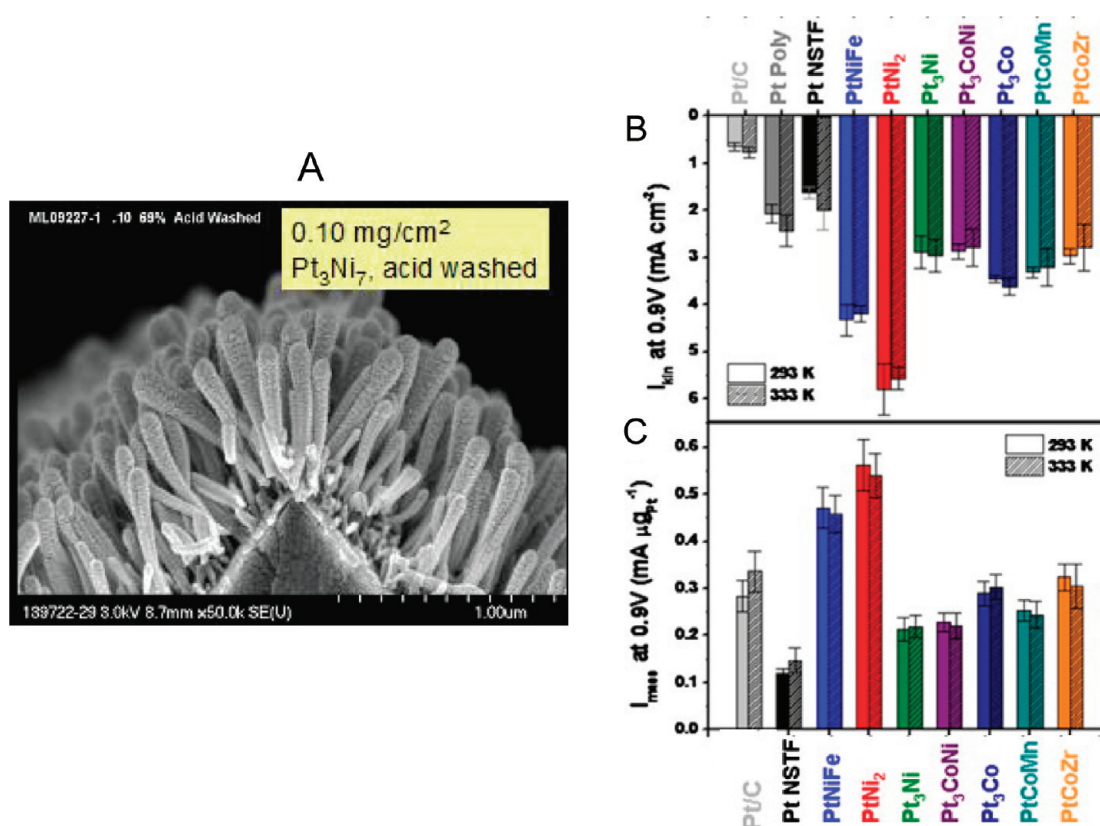

Figure 11. (A) SEM images at originally 50 k magnification, of the NSTF catalysts with Pt_3Ni_7 coating after acid washing. Reprinted with permission from ref 200. Bar graphs of the ORR specific activity (B) and mass activity (C) on NSTF catalysts, compared with polycrystalline Pt at 0.9 V. The single-color bars represent the value at 293 K, and the accented bars represent 333 K. Reprinted with permission from ref 201.

support systems have been reported in the literature. Details will be found in the next section.

(v) One approach is the use of supportless catalysts, for example, Pt-black, or sputter-deposited Pt[185−187] (e.g., the 3M NSTF-approach[188] which we will discuss in detail in section 4.1).

In the previous discussion, we outlined the carbon corrosion occurring under conditions of high potentials. Under these conditions, certainly also reaction 5, the dissolution of platinum will take place. It is known that Pt dissolution occurs at significant rates when it is subjected to continuous oxidation− reduction cycles during voltage cycling.[189] This effect is actually known quite well from past PAFC research. For a summary of the PAFC finding, the reader is referred to the excellent overview in ref 190.

In this study, it was also shown for the first time that Pt coarsening occurs by two different mechanisms: first, so-called Ostwald ripening of Pt on carbon, which occurs on a nanometer scale leading to the well-known particle growth of the nanoparticles to up to 6 nm; second, dissolution of Pt

species into the electrolyte (or ionomer phase) occurring on a micrometer scale with transport of the dissolved species into the membrane until a point where they will be chemically reduced by crossover hydrogen and precipitated.[190] At least under the conditions of ref 190, it is estimated that both processes occur to similar extent. Visualization of deposited Pt bands in the membrane or next to the membrane-cathode interface using SEM, TEM, or electron-probe microanalysis can be found, for example, in refs 191, 178, 179, and 190.

In addition to the performance improvements for Pt-alloys, dealloyed Pt-alloys, or other monolayer core shell nanoparticles as discussed in section 2.2, several studies also proved its higher stability under potential and start−stop cycling conditions in both low and high temperature PEFCs.[149,151,179,192] Hasché et al. report about up to 5-fold better surface-specific current densities for their dealloyed Pt_3Cu, Pt_3Ni, and Pt_3Co catalysts vs pure Pt, respectively, after up to 10 000 voltage cycles between 0.5 and 1 V at room temperature. Hartnig and Schmidt demonstrate in a PEFC operating at 180 °C that after 150 simulated start−stop cycles, Pt-alloy cathodes show ∼30 mV less increase in overpotentials as compared with pure Pt catalysts. Similar improved stabilities have been reported from the Adzic group in the field of their metal core−Pt monolayer catalysts.[192−194] Recent results from the same group describe the sustained high kinetic activity of Pt-hollow nanocrystals with contracted lattice formed by the so-called Kirkendall effect (basically the faster solid-state diffusion of 3d metals as compared with Pt, which is supposed to be the reason for the instability of, e.g., some core−shell systems).[195] Another promising approach represents the core−shell system with Au core and $FePt_3$ shell supported on carbon, which at least in 0.1 M $HClO_4$ solution at 20 °C retains its high kinetic activity after 60 000 potential cycles to 1.1 V, more than an order of magnitude more than Pt/C.[143] One of the drawbacks, however, of Fe-containing catalysts may be their deleterious effect on membrane and ionomer stability when traces of Fe are dissolved. In summary, there appears to be hope that these catalysts, which mainly have been characterized outside a fuel cell, will find their way into gas-diffusion electrodes and maintain their positive durability properties also in realistic fuel cell testing.

As already mentioned, one of the major drawbacks of nanoparticles, however, is their inherent instability when compared with extended Pt surfaces (e.g., Pt-black, sputtered Pt layers, or the 3M NSTF catalyst approach). Properties of these systems will be discussed in more detail in the next sections.

4. NEW MATERIALS

4.1. Extended Pt-Black Type Surfaces. Since the report of Debe et al. in 1994, 3M Company has been developing nanostructured thin-film (NSTF) catalysts.[196,197] This type of catalyst consists of a single layer of crystalline whiskers of about 1000 nm in length, about 50 nm in diameter and with an areal number density of 3–4 billion cm^{-2}.[198] These whiskers are obtained by temperature annealing of a vacuum-deposited organic pigment (N,N-di(3,5-xylyl)perylene-3,4:9,10bis-(dicarboximide), referred to as perylene red; CAS no. PR149).[196,197,199] Then the catalyst is completed by deposition of the desired catalyst (Pt or Pt-alloy) on these support structures in a single physical vapor deposition or sputter deposition step (see Figure 11A).

The crystalline whiskers have shown high thermal, chemical, and electrochemical stability under fuel cell operation conditions. The roughness of the catalyst coating on the whiskers can vary from very smooth to very rough, and it depends on the deposition conditions and the metal elements. One important characteristic of this kind of catalyst is that for the same Pt loading, the electrochemical surface area is smaller than Pt/C layers.[188,202] The NSTF catalyst does not need another electronic conductor in addition to carbon, and due to the high ion diffusion within the catalyst layer (less than 1 μm), the addition of ion conductive ionomer as Nafion is not required,[198] an effect already described and discussed.[203] The NSTF-based electrocatalysts provide up to 10 times higher area specific activity toward the ORR than conventional Pt-supported catalysts and 50% higher mass activity, using current standard NSTF whisker supports (Figure 11B and C)[188,204,205]

The activity enhancement of this catalyst toward the ORR is not fully understood. It is considered that parameters such as the nature of metal/support interactions, the improved ionic transport, or the morphology of the Pt layer may be the origin of this enhancement in catalytic activity. As was mentioned before, specific surface orientation and surface defects are known to have a large influence on ORR, and for that reason, the morphology of the surface is considered the main source of the catalytic activity of the NSTF.[202] An important contribution in the analysis of the morphology of NSTF structures is described in ref 202. The authors performed physical and electrochemical characterization of three compositionally different NSTFs: Pt, PtRu, and PtNiFe. One of the most significant conclusions of this work is the fact that the NSTF catalyst presents homogeneously distributed oriented whisker-ettes (small secondary whiskers growing from a main whisker) with a fcc metal crystal structure differing from the conventional carbon-supported electrocatalysts. In addition, the authors conclude that even though the PR149 support does not play a role in the electrocatalytic process, it has a strong influence on the metal whiskerette population density and growth mechanism.[202]

Another approach to explain the higher specific activity of the Pt-black type extended NSTF catalyst could be the influence of particle size on the ORR activity (see Figure 12). Very recently, Nesselberger et al.[206] have shown that in contrast to previous reports, the specific activity[125,207] of the ORR rapidly decreases with the particle size, going from polycrystalline Pt to unsupported Pt black particles, and HSA carbon supported Pt NPs, In addition, the authors have shown that the mass activity of the ORR does not exhibit a maximum at one specific particle size/dispersion but increases with the electrochemical surface area of the catalyst. Especially when comparing different studies on the particle size effect for the ORR, it becomes quite obvious that different ways of analyzing the ORR activity (e.g., IR-correction, values from anodic or cathodic sweeps, correction for base CVs, etc.) will result in quantitatively different results. Quite interestingly, however, normalizing the values from the different studies to an arbitrary specific surface area (as in Figure 12, we normalized the different activities by the activities at 20 m^2/g_{Pt}). It becomes obvious that the activities follow a master curve for ORR activities as a function of the specific surface area (see Figure 12).

This particle size effect can be attributed to the shift in the potential of zero total charge to lower values as the particle size (specific surface area) diminishs (increases), that is, smaller particles with higher amounts of undercoordinated surface
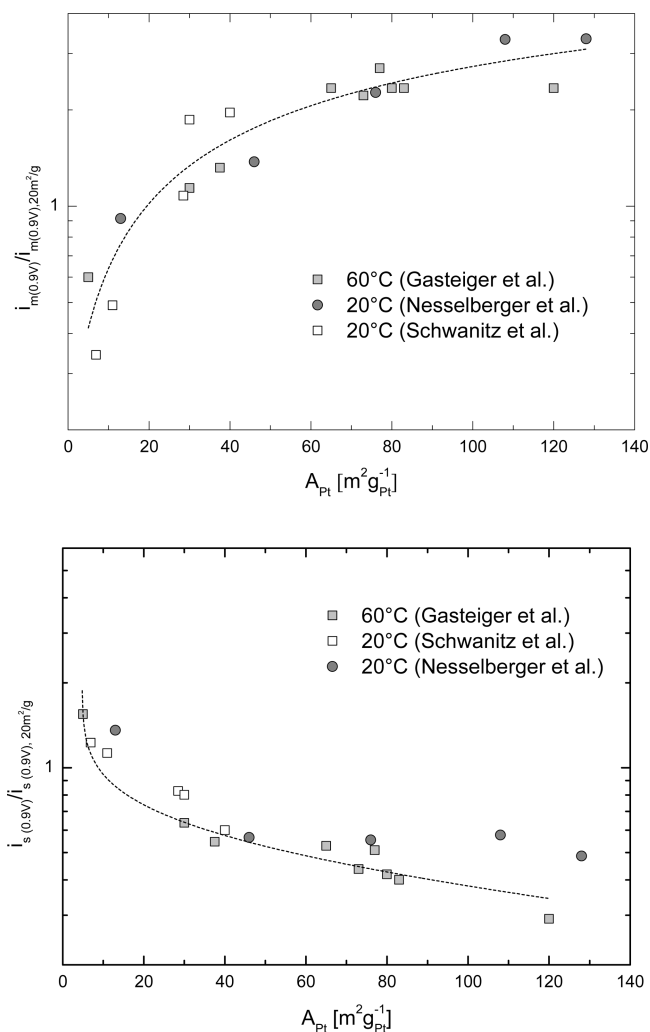
Figure 12. Specific ($i_{s(0.9\,V)}$) and mass ($i_{m(0.9\,V)}$) activity at 0.9 V toward the ORR on different Pt catalysts normalized to the respective current values at 20 m^2/g$_{Pt}$ specific catalyst surface area in the particle size range from ~1 nm to ~30 nm and on extended Pt-black type surfaces. Data in the plot are extracted from RDE measurements by Gasteiger et al.[125] (60 °C, 0.9 V, 5 mV/s, data taken from anodic sweeps, 1600 rpm, 0.1 M HClO$_4$, Pt/C, Pt-black, and Pt-poly), Schwanitz et al.[187] (20 °C, 0.9 V, 5 mV/s, 1600 rpm, data taken from cathodic sweeps, 0.1 M HClO$_4$, sputtered Pt particles and layers), and Nesselberger et al.[206] (20 °C, 0.9 V, 1600 rpm, anodic sweeps, base CV- corrected, Pt/C catalysts, Pt-black).

atoms become more oxophilic as compared with larger particles or Pt-layers.[207]

In terms of catalytic activity improvement in recent years, the major contribution comes from the works of the group around Debe and Atanassoski.[188,198,205,208−213214] In a very recent report, 3M showed that by using the Pt$_{68}$Co$_{29}$Mn$_3$ NSTF catalyst, it is possible to exceed the previous 2015 target of the U.S. Departmen of Energy (DOE 2015) of 0.2 g$_{Pt}$/kW in a full-size short stack with 0.05 mg/cm^2 of precious group metal on the anode and 0.1 mg/cm^2 on the cathode. Although the new DOE 2015 target of 0.125 g$_{Pt}$/kW (down from 0.2 g$_{Pt}$/kW) with a total of 0.125 mg/cm^2 of precious metal group per square centimeter of MEA requires further work, new binary and ternary alloys are being developed.[215] The authors have investigated a large series of NSTF-Pt$_x$M$_y$N$_z$ alloy catalysts (M, N = Ni, Co, Zr, Hf, Fe, Mn) covering a wide range of alloy

compositions $(0 \leq x, y, z < 1)$.[204,205,208,212,214] The ORR activity of PtCo weakly depends on the Co content; however, it showed a loss of bulk Co from the lattice, resulting in a loss of activity.[213] On the other hand, PtNi catalyst shows a surprisingly sharp dependence of ORR mass activity. The electrode with Pt$_{0.27}$Ni$_{0.73}$ shows 60% higher mass specific activity toward the oxygen reduction reaction than the other alloy compositions but suffers from lower values of limiting currents due to dealloying and subsequent dissolution of the excess Ni into the membrane and its effect on water management. In addition, the slight increase in the Ni content (Pt$_{0.75}$Ni$_{25}$) shows a drop in the mass activity.[204,208,216]

In terms of durability, the DOE 2015 targets are that ORR activity and surface area will each drop <40%, and the performance at 1.5 A/cm^2 will drop less than 30 mV from initial levels. The PtCoMn NSTF catalyst from 3M under operation conditions (potential hold at 1.2 V vs RHE for nominally 400 h under 150 kPa H$_2$/N$_2$ at 80 °C; loading at the anode, 0.05 mg/cm^2; loading at the cathode, 0.15 mg/cm^2) have shown surface area losses of 10% while specific activity was unchanged and the performance at 1.5 A/cm^2 dropped only 10 mV. These results were expected because of the absence of support corrosion.[215] Therefore, it appears that the NSTF catalyst approach may be currently the most promising to meet final catalyst activity and durability targets as defined in Table 1 (please note that 2011 status values represent results reached using 3M's NSTF catalysts).

4.2. Nonprecious Metals. Numerous efforts are being developed to replace Pt-based catalysts in PEFCs due to the high cost and abundance of the metal. Recent developments in nanotechnology and materials science have raised high expectations in the design and synthesis of alternative new nonprecious-metal catalysts with high activity and practical durability for the ORR in PEFCs. In the most recent two decades, some promising Pt-free catalysyts for ORR have been studied intensively: nonprecious-metal chalcogenides;[217−222] carbides;[223−226] nitrides;[227,228] organometallic compo-nents;[229−234] and very recently, N-doped carbon catalyst with a graphitic structure, such as CNTs and graphene.[235−240]

Among these materials, nonprecious or transition metal chalcogenides have received the attention of researchers to replace the Pt catalyst since the 1970s. Baresel et al.[241] was one of the first to report the high electrocatalytic activity of CoS toward the ORR. Although the activity and stability of the transition metal chalcogenide nanomaterials toward the oxygen reduction reaction are still far from the requirements for practical fuel cell applications, significant progress has been reached since the Chévrel-phase Ru$_2$Mo$_4$Se$_8$ was reported in the pioneering work by Alonso-Vante and Tributsch,[242] showing activity comparable to Pt catalysts toward the ORR (Figure 13A). However, the synthesis procedure for Chévrel-phase catalysts is complicated and costly. In this regard, several synthetic routes of late transition metal chalcogenide catalyst have been designed, namely, chemical vapor deposition,[243−246] sonochemical synthesis,[247−252] surfactant/capping-assisted soft synthesis,[253−258] and hydrothermal/solvothermal,[259−264] among others. In particular, our attention is drawn to the so-called "soft-synthetic routes" over the physical method because they provide a simple route to obtain the catalyst with desirable composition, shapes, and sizes. These catalysts, mainly consisting of metal atoms (Fe, Co, Ni), have regained interest because of their low cost, good ORR activity, high methanol and halides tolerance, and facile synthesis. Among the
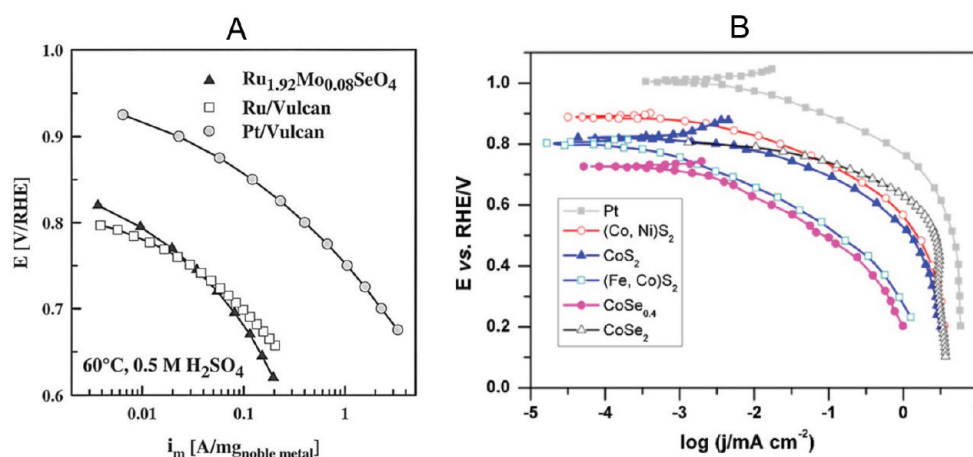
Figure 13. (A) (a) Mass-specific Tafel plots for $Ru_{1.92}Mo_{0.08}SeO_4$ (40 $\mu g_{Ru}/cm^2$) (triangles), Ru/Vulcan (14 $\mu g_{Ru}/cm^2$) (squares), and Pt/Vulcan (14 $\mu g_{Pt}/cm^2$) (circles). Reprinted with permission from ref 221. (B) Comparison of the polarization curves in 0.5 M H_2OS_4 of Pt, $CoSe_{0.4}$,[268] (Fe,Co)S_2,[265] (Co,Ni)S_2, CoS_2 thin films[269] and cubic-phase $CoSe_2$/C (20 wt %) powder[222] in a RDE configuration at room temperature. Reprinted with permission from ref 219.

chalcogene elements, O, S, Se, and Te are the most intensely investigated.

The nonprecious metal chalcogenides show as a general characteristic a half-wave potential, $E_{1/2}$, around 0.65 V vs RHE, which is lower than that of Pt-based catalysts (0.87 V vs RHE). The H_2O_2 maximum production at lower potentials is less than 4%, which suggests an overall four-electron transfer reaction pathway. Feng et al.[219,220,222] prepared test nanoparticles of Co_3S_4 and $CoSe_2$ supported on carbon. The 20 wt % Co_3S_4/C catalysts showed ORR electrocatalytic activity in 0.5 M H_2SO_4 with the onset potential at ~0.7 V vs RHE. Susac's group[265−268] investigated the activity and stability of CoSe, CoS_2, and FeS_2 thin films with thicknesses of ~0.4−0.5 μm. In all the cases under study, its high activities toward the ORR and high stabilities at PEFC cathode potentials are demonstrated, although the corresponding open-circuit potentials are still lower than for Pt (Figure 13B).

In terms of mechanistic understanding, it is accepted that in the Chévrel-phase the oxygen molecules adsorption takes place at the Mo center, and later, the adsorbed oxygen is reduced on Ru atoms acting as the catalytic center for the oxygen reduction reaction (Figure 13a). DFT calculations suggest that for the chalcogen-containing surfaces, a linear relationship describes the correlation between the center of the d-band of the surface metal atoms and the adsorption energies of the ORR intermediates.[217]

On the basis of DFT calculations, Tripsaris et al. suggest that the methanol tolerance of transition metal chalcogenides can be attributed to the relatively high energy barrier for the initial dehydrogenation of methanol compared with the pure surfaces.[217] Experimentally, it was found that the activity of the ORR on Ru-chalcogenides is not affected by the presence of methanol,[219,221,270,271] and it was suggested that even the adsorption of methanol is hindered on the highly OH-covered surfaces at cathode potentials.

Although carbon nanotubes have been used as supports for a nanoparticle metal catalyst, it has been recently demonstrated that surface-modified carbon nanotubes, mesoporous carbon, and graphene show ORR electrocatalytic activities in alkaline[235,272] and acidic media.[238,273−276]

N-doped carbon nanostructures have special electronic and mechanical properties due to the conjugated nitrogen lone-pair electrons and the graphene p-system.[239,276,277] The strong electron affinity of the nitrogen dopant effectively weakens the O−O bond. As a result, the adsorption of O_2 can significantly enhance the rate of the ORR. It is considered that the high rate of O_2 reduction is related to the content of pyridinic nitrogen in the dopant. In this sense, some authors support the idea that the N-doped carbon materials have an intrinsic catalytic activity of their own,[278] but other authors suggest that the high catalytic activity of the N-doped carbon nanostructures is mainly due to the interaction of the nitrogen termination with the Fe or Co center coming from the synthesis of the material. On the other hand, it is suggested that iron just influences the formation of the active site through the carbon nanostructure growth mechanism. It has also been shown that the increase in the graphitic defects and thereby also oxygen-containing groups improves the ORR.[279] Kruusenberg et al.[238] also showed that the catalytic activity of the carbon nanotubes toward the ORR depends on the purification treatment.

Although most of the studies of ORR on graphene have been done in alkaline media,[235] very recently, N-doped graphene exhibited significantly high ORR activity going through a four-electron pathway.[236] DFT simulation shows that the active sites on the N-graphene depend on spin density and atomic charge distribution. The N-doping introduces unpaired electrons to the graphene and leads to the asymmetry spin density that changes the atomic charge distribution on it. This change in the charge distribution creates the active sites on the graphene which can be considered as the cause for the high electrocatalytic ORR activities.[237]

The combination of both above mentioned catalysts, N-doped carbons and chalcogenides catalyst,[280,281] have being tested for the ORR reduction reaction in alkaline media exhibiting similar catalytic activity but better stability than Pt. Unfortunately, to our knowledge, this hybrid catalyst has not being tested in an acidic environment.

4.3. Organometallic Catalyst.
The first studies regarding the use of organometallic components as catalysts in fuel cells are reported in the 1960s in pioneering studies by Jasinski.[282,283] These studies showed that non-noble metal catalysts based on Co-phthalocyanine are active toward the oxygen reduction reaction. The extended delocalized π-systems, for example, in phthalocyanines, are able of undergoing fast

redox electron transfer reactions and acting as mediators in electrochemical processes as the oxygen reduction reaction.

These studies have attracted the attention of many others groups, which extend the research to organometallic N^4-macrocyclic components. Although the initial and most extended studies are found on macrocycle complexes of transition metals, the research on non-precious metal has expanded from porphyrin-type materials to macrocycles and noncyclic materials (Figure 14).[284−290] Although the first
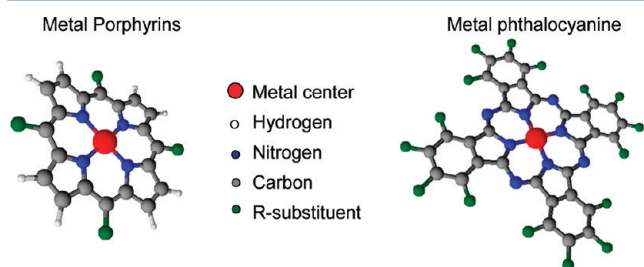

Figure 14. Structure model of some of the most common metal organic complexes.

results in these kinds of systems showed that the catalyst stability and activity toward ORR is improved by subjecting the N^4-macrocyclic sample to thermal pretreatment up to 500−600 °C in an inert gas (N_2 or Ar), the structure of the resulting catalytic site and the reaction mechanism was under debate for more than two decades.

Probably one of the most important contributions in the field was made by Yeager's group, who demonstrated that the catalytic active site is not formed during the heat treatment but is self-assembled afterward during contact with the electrolyte that dissolves metal particles, which had been generated during pyrolisis.[291−293] The authors by then conclude that the catalytic activity toward the ORR in acid medium requires four crucial components: the nitrogen precursor, the transition metal precursor (e.g., Fe or Co), the carbon support, and the temperature pretreatment of the material at relatively high temperature. The last step leads to the formation of N functionalities on the carbon support and also induces the reduction of the metal ions. This report represented a crossing point for the preparation of nonprecious metal-based catalysts for the ORR: (i) the nitrogen and metal precursor are part of the same molecule (N^4-macrocyclic components) and (ii) metal and nitrogen belonged to two different molecular precursors.

In addition to the studies of Yeager's group, one of the major contributions to this research was done by the group of Dodelet and co-workers.[285,289,290,294−302] They demonstrate the presence of two catalytic sites, Fe−N^2/C and Fe−N^4/C;[303] however, the Fe−N^2/C catalytic sites are more electrochemically active than the Fe−N^4/C ones.[294,303,304] An explanation for that is that the Fe−N^2/C catalytic sites have the property to reduce O_2 primarily to water. Another important later observation of the authors was the effect on the apparent number of electrons transferred during ORR as a function of the carbon support.[289]

Regarding the electrotransfer mechanism during the ORR, the apparent number of electrons (n) has been reported for several organometallic N^4-macrocyclic compounds after pyrolisis.[285] In particular, the ORR reduction on Fe-based catalysts occurs mainly through a four-electron transfer, and the

main product is water, whereas for Co-based precursors, the main product is H_2O_2 and n = 2. Although the exact mechanism of the ORR is not as elucidated as in the case of the metal catalyst, the reduction of O_2 to water may occur directly with the transfer of four electrons (4e) but more likely proceed to the formation of H_2O_2 with the transfer of two electrons, followed by the transfer of another two electrons during a subsequent reduction to water.[294]

In terms of adsorption sites and structures, it is proposed that the O_2 adsorption takes places between the transition metal and terminal oxygen atom in an on-top type configuration. However, Yeager et al. also proposed the bridge oxygen adsorption, whereas a trans configuration has been proposed to occur with dimeric cobalt dioxygen complexes.[285] Probably the most important difference between the Fe-based catalyst and the noble metal catalyst (such as Pt) is the formation of the intermediate illustrated in Figure 15 and formed by the
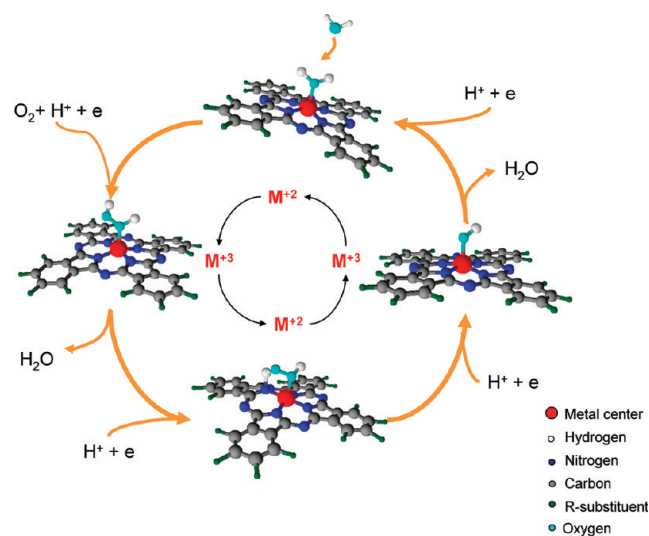

Figure 15. Tentative model of the reaction step mechanism in the ORR in a N^4-metallorganic catalyst.

interaction of the HOOH and Fe and the nitrogen lone pair orbitals in the N_4 structure. This bridge-type structure provides a path for direct reduction to water on Fe-based catalysts.

In Figure 16, Lefevre et al. illustrate the comparison in activity under the same conditions of nonprecious metal catalysts and precious metal catalysts inside a PEFC. It is shown that even if the nonprecious catalyst loading of ∼5 mg cm^{-2} is larger than that for Pt (0.4 mg cm^{-2}), the limiting factor for the Pt loading is materials cost, and the limiting factor for nonprecious metal loading is electrode thickness. The authors report that for the Fe-based catalyst, an increase in the thickness beyond ∼100 μm produces undesirable mass transport losses and the decay of the power density. It should be noted, however, that in this study, for the first time, this type of catalysts inside a GDE in a PEFC produced similar activities as compared with state-of-the-art PEFC MEAs using a Pt/C catalyst. The results from ref 302 are clearly influential for the R & D of these catalyst types, since many new research projects have been triggered through this exceptional publication.

More recently, Zelenay's group contributed to the study of organometallic catalysts.[284,305−307] The authors performed activity and durability tests using cobalt polypyrrole and polyaniline, iron, and cobalt catalysts. In the first case, the
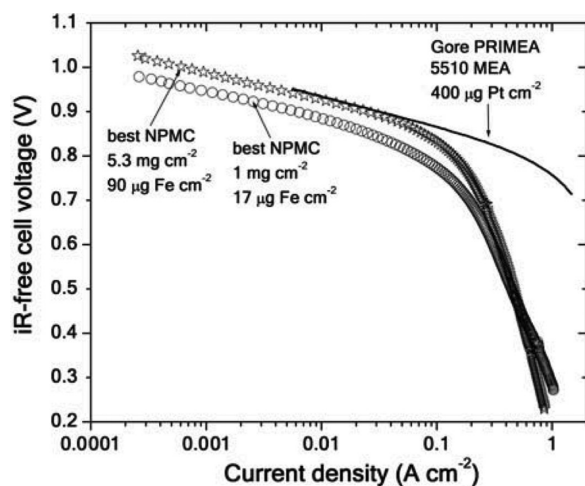
Figure 16. Comparison of the best nonprecious metal catalysts in 302 with a Pt-based catalyst. Polarization curves from H_2-O_2 fuel cell testing ($P_{O_2} = P_{H_2}$ = 1.5 bar, 80 °C, 100% relative humidity) are shown. Loadings: 1 mg cm^{-2} (circles), 5.3 mg cm^{-2} (stars). Comparison with a state-of-the-art Gore PRIMEA 5510 membrane electrode assembly (MEA; W. L. Gore & Associates, Newark, Delaware, USA) with ~0.4 mg$_{Pt}$ cm^{-2} at cathode and anode (black line). The actual Fe content in our catalyst is 1.7 wt %, resulting in a Fe loading of 17 mg cm^{-2} for a catalyst loading of 1 mg cm^{-2}. Open circuit voltages are 1.03, 1.03, and 1.01 V for the MEAs using 17 and 90 mg$_{Fe}$ cm^{-2} and 400 mg$_{Pt}$ cm^{-2} at the cathode, respectively. Reprinted with permission from ref 302.

authors show that cobalt polypyrrole catalyst enables power densities of ~0.15 W cm^{-2} (cobalt loading 6 × 10^{-2} mg/cm^2; Co-specific power density of 0.4 g$_{Co}$/kW) in H_2-O_2 fuel cells without catalyst degradation after more than 100 h of operation. In a standard Pt/C catalyst (TKK) with 47% loading and a Pt surface area of ~75 m^2/g$_{Pt}$, Gasteiger et al.[308] reported a power density at 0.65 V of 0.71 W/cm^2, translating into a Pt-specific power density of 1.1 g$_{Pt}$/kW; however, identical performance was obtained from the same authors, but for a reduced anode loading of 0.05 mg$_{Pt}$/cm^2 [309] which is a considerable decrease in the Pt-specific power density to a value of 0.63 g$_{Pt}$/kW at 0.65 V.

In the second study, polyaniline was used as a precursor for a N-carbon template for high-temperature synthesis of catalysts incorporating iron and cobalt. It is important to highlight that the H_2O_2 yield measured with PANI-derived catalysts remains below 1% at all potentials and shows little loading dependence. In addition, the authors report very promising performance stability of the PANI−FeCo−C. The authors reported just an average current-density loss of 18 μA h^{-1} in 700 h of fuel cell operation conditions at a constant 0.4 V and 80 °C, which is comparable to the losses on 100 h life test under the same conditions of an E-TEK 20 wt % Pt/C catalyst.[284]

4.3. New Support Materials. Stability and Electronic Effect. The performance and durability of low-temperature fuel cells seriously depend on catalyst support materials. The support ensures electronic conduction pathways, homogeneous dispersion of Pt-based catalyst particles and ionomer, and gas transport in the formed porous catalyst layer. Catalysts supported on high-surface-area carbons are widely used in low-temperature fuel cells. However, the corrosion of carbonaceous catalyst−support materials,[310] such as carbon black, has been identified as one of the causes of performance degradation of fuel cells since the times of the large PAFC development

activities in the 1970s and 1980s.[166] Only since the late 1990s has this important degradation mode also been recognized in the development of PEFCs, in particular under repeated start−stop cycles or high-potential conditions.[311] Since then, many attempts have been performed to either stabilize carbon support materials or find new materials with improved properties. The quest for new support materials should be guided by the following requirements, which are summarized below:

(i) Electronic conductivity of the support material is assumed to be above 0.1 S cm^{-1} in the range of the device operation temperature (−20 to 80 °C). This value arises from the approximation that commonly used carbon supports have an electrical conductivity of around 2−3 S cm^{-1}, whereas the proton conductivity of the ionomer in the catalyst layer is only 0.02 S cm^{-1} at 50% RH.[167] Thus, an electrical conductivity above 0.1 S cm^{-1} (i.e., ~20−30 times lower than commonly used carbon materials) should be sufficient without imposing Ohmic losses in the catalyst layer.

(ii) The support material should be able to form porous structures with pore sizes larger than 25 nm in the catalyst layer. Current electrode materials (carbon blacks) have porosities of 80% (exclusive the ionomer phase, 50−60% inclusive the ionomer) with main pore sizes in the range of 20−100 nm. For air in porous catalyst layers, Knudsen diffusion (i.e., gas molecule−pore wall interactions dominate over molecule−molecule interactions with $d_{molecule} < d_{pore} < \lambda_{mean}$ where d represents the molecule and the pore diameter, and λ_{mean}, the mean free pathway of diffusing gas, respectively) becomes dominating at pore diameters below 25 nm under typical PEFC operating temperatures and pressures.[312] As a consequence, the required pore sizes created with a new support in a catalyst layer should be larger than at least 25 nm.

(iii) Dissolution of the support material (e.g., metal cations) under fuel cell relevant conditions must be excluded. With respect to cationic dissolution products, only 10% of the total H$^+$ sites of the membrane/ionomer can be allowed to exchange without significant performance loss (losses of a maximum of 10 mV at 1 A cm^{-2} vs uncontaminated MEAs) during the MEA lifetime.[313] Using standard values from state-of-the-art MEAs (0.5 mg$_{Pt}$ cm^{-2} using 50% Pt/C, ionomer: carbon ratio of 1:1, and a 50 μm EW1100 membrane), the total number of exchangeable H$^+$-containing sites are on order of ~10^{-5} mol$_{H^+}$ cm^{-2}, that is, a maximum of ~10^{-6} mol$_{H^+}$ cm^{-2} can be exchanged without significant performance losses. Consequently, over a lifetime of a PEFC, only 10^{-6} mol cm^{-2} metal ions from the support are allowed to be dissolved into the membrane and ionomer phase.

(iv) Reasonable support materials should provide a BET surface area of more than 50 m^2 g^{-1}, which is at least in the range of graphitized carbon blacks, to obtain a high Pt dispersion (ratio of surface atoms to total number of atoms) of >30% in the final catalyst.

(v) Low-cost materials are desirable as support. The prize of possible support materials should not significantly exceed the value of high-surface-area carbon (or even advanced graphitized carbon) of ~15 € kg^{-1} (10 kg range low volume cost).[314] The cost questions, however, must be

evaluated from case to case in connection with cost-vs-lifetime considerations and should not a priori exclude promising materials.

During the past ten years, several research groups started to look for corrosion-resistant ("carbon-free") support materials for Pt-based electrocatalysts in PEFCs. For this reason, several conducting and semiconducting materials have been studied as electrocatalyst support and cocatalyst materials for PEFCs in acidic media. Especially, conductive oxides gained much interest during the that time because of their potentially high stability in acidic environments and unique chemical and physical properties related to the multivalence of transition metal oxides, but also, carbides, nitrides, and conductive diamonds have promising properties as electrocatalyst support material.

Carbides. Different transition metal nitrides and carbides were investigated by various research groups,[209,315,316] because of their noble-metal-like behavior toward some chemical and electrochemical reactions, including oxidation of hydrogen, CO, and alcohols, and reduction of oxygen.[317−319] Medium activity as an electrocatalyst and certain solubility was found, especially at high cathodic potentials. But recently, tungsten carbides (WC, W_2C) have received considerable attention as support material for electrocatalysts because of their unique resistance to CO poisoning[320] and their platinum-like electronic structure (near the Fermi level, WC resembles the electronic density of states of Pt).[317,321]

Cui et al.[322] demonstrated an 87 mV lower onset of CO oxidation of their prepared Pt/WC/C catalyst (C denotes the GDL material) compared with a traditional Pt/C (HiSpec 4000) in CO stripping experiments, shown in Figure 17.
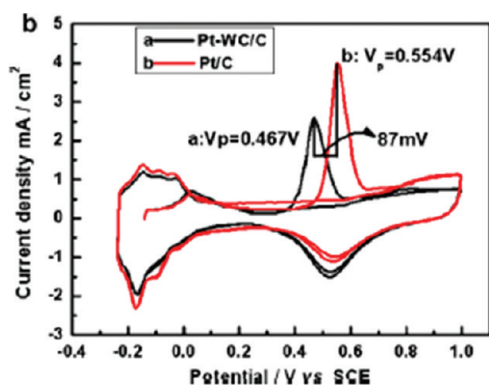

Figure 17. CO-stripping data on Pt/C and Pt/WC in 0.5 M H_2SO_4 at a scan rate of 20 mV s^{-1}. Reprinted with permission from ref 322.

Through surface electrostatic potential calculations, they state an electron-donating effect, which at low potentials would help to avoid CO adsorption and show at high potentials an enhanced CO oxidation. Chhina et al.[323] demonstrated the ORR activity of Pt/WC electrocatalyst prepared on a carbon-based GDL to remain high even after accelerated oxidation tests by potential cycling (10 000 cycles) between 0.6 and 1.8 V at 80 °C, but the ORR activity was extremely poor after the same test procedure for Pt/C. Further, the electrochemical stability of WC could be improved in acidic electrolyte by adding Ta, Fe, Co, or Ni.[224,324] Ishihara[224] demonstrated a high stability of their sputter-deposited catalyst support WTaC. The passivity of the tantalum compound offers corrosion protection

for the WC through the formation of a hydroxide layer during cyclic voltammetry.

To make high-surface-area tungsten carbide, different synthesis routes were investigated. Chhina et al. showed magnetron sputtering of tungsten carbide and platinum to be one of the most promising routes.[325] Another approach was recently published by Jones's group, who prepared tungsten carbide microspheres[326] using a simple hydrothermal method. These microspheres exhibit a very high surface area and an exceptionally high electrochemically active surface area stability compared with the commonly used Pt/C electrocatalysts for PEFC application.

One of the drawbacks of carbides (and nitrides) may be their thermodynamic instability under oxidative environments as present in a PEFC cathode. Although generally assumed to be "stable", they eventually are transformed to the transition metal oxide, which for most metals is the only thermodynamically stable compound under these conditions. Therefore, on the basis of thermodynamic and electrochemical stabilities,[175] conducting (transition) metal oxides seem to be a potentially more suitable class of materials for electrocatalyst supports.

Conductive Metal Oxides: Stability and Effects. Durability of new support materials under severe fuel cell operation conditions is one of the most important issues to be improved to create a MEA with extended lifetime. Sasaki and co-workers[327] conducted thermochemical calculations to determine stable substances under fuel cell relevant conditions (potential of 1.0 V_{SHE}, pH = 0, and 80 °C). According to their results (shown in Figure 18), W, Ti, Sn, Nb, Ta, Sn, and Sb are stable as oxides, hydroxides, or metals under these conditions.

Even without these calculations, the most work in recent years has been carried out on the oxides of titanium;[328−330] tin;[331,332] tungsten;[333−335] and in general, the valve metal oxides,[336,337] such as ZrO_2,[338,339] ZrO_xN_y,[227,228] Ta_2O_5,[333] TaO_xN_y,[340] and HfO_xN_y.[341,342] The greatest progress has been made by improving the electrical conductivity by doping or modifications of the oxide surface;[343] increasing the surface area through nanostructures, mesospheres etc.; and mainly by a deeper understanding of metal−support interactions and particle size influences.

Recently, Eguchi's group[344] found that SnO_2 influences the oxidation and reduction of oxide-supported Pt-based catalysts. It seems that the adsorption/desorption of oxygen on Pt and the formation/reduction of PtO_x above 0.6 V is suppressed. Alonso-Vante and co-workers[345,346] investigated changes in electronic properties of both platinum and oxide supports, induced by the so-called strong metal−support interactions (SMSI). Lewera et al.[345] found at least two factors that induced a change in the electronic properties of Pt: (i) the charge transfer from the oxide to Pt atoms and (ii) a change in the lattice parameter due to alloy formation.

In Figure 19, the observed shift in the binding energy of the Pt 4f level from XPS measurements is shown, which suggests that there is an increased electron density on the Pt surface atoms or at least a modified surface electronic structure of Pt, which is said to result in a weakening of the interaction between Pt and intermediate surface species, resulting in more active sites for O_2 adsorption. These results might be one explanation for the improved corrosion resistance of Pt and the expected enhanced catalytic activity toward the ORR.

In parallel, some studies have been carried out to evaluate the influence of catalyst particle size (e.g., Pt) on the catalytic activity of supported electrocatalysts. Hayden's group[347−349]

Metal-H₂O system at 80°C
Molality m ($m = 10^{-0}$ mol/kg H₂O), pH = 0
Cathode E_h (vs. SHE) = 1.0 V

Li	Be
Li^+	Be^{2+}

B	C	N	O	F
H_3BO_3 (a)	CO_2 (a) / CO_2 (g)			

Na	Mg
Na^+	Mg^{2+}

Al	Si	P	S	Cl
Al^{3+}	H_2SiO_3 (a) / H_4SiO_2	$H_4P_2O_7$ (a)	HSO_4^-	

K	Ca	Sc	Ti	V	Cr	Mn	Fe	Co	Ni	Cu	Zn	Ga	Ge	As	Se	Br
K^+	Ca^{2+}	Sc^{3+}	TiO_2	VO_4^-	Cr^{3+}	Mn^{2+}	Fe^{3+} (Fe_2O_3)	Co^{2+}	Ni^{2+}	Cu^{2+}	Zn^{2+}	Ga^{3+}	GeO_2	$HAsO_4$ (a)	H_2SeO_3 (a)	

Rb	Sr	Y	Zr	Nb	Mo	Tc	Ru	Rh	Pd	Ag	Cd	In	Sn	Sb	Te	I
Rb^+	Sr^{2+}	Y^{3+}	ZrO^{2+}	Nb_2O_5	MoO_3		RuO_2	RhO_2 (g)	PdO_2	Ag^+	Cd^{2+}	In^{3+}	SnO_2	Sb_2O_3	$Te(OH)_3^-$ (H_2TeO_4)	

Cs	Ba		Hf	Ta	W	Re	Os	Ir	Pt	Au	Hg	Tl	Pb	Bi	Po	At
Cs^+	Ba^{2+}		HfO_2	Ta_2O_5	$O_2W(OH)_2$	ReO_4^-	OsO_4 (a) (OsO_2)	IrO_2	Pt	Au		Tl^-	Pb^{2+}	Bi_2O_3		

Figure 18. Most stable substances under typical PEFC cathode conditions at 80 °C, derived from pH-potential diagrams thermochemically calculated. Reprinted with permission from ref 327.
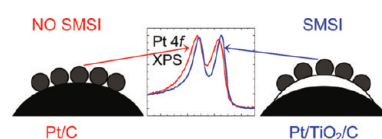

Figure 19. XP spectra of the Pt 4f region registered for Pt/C (blue line) and Pt/TiO₂/C (red line). A significant down-shift of Pt 4f BE can be observed when Pt is deposited on an oxide−carbon composite. Reprinted with permission from ref 345.

studied the particle size effect on supported electrocatalysts with the help of a novel high-throughput technique and compared the precious metal/C with precious metal/TiO$_x$ electrocatalysts (Au and Pt) in terms of catalytic activity for the ORR, depending on the support and catalyst particle size. For both supports, they found the catalytic activity toward ORR rapidly decayed for catalyst particle sizes below 3.0 nm, with the substrate influencing kinetics of surface redox couples and, therefore, the adsorption of anions and water. Similar particle size and support effects were demonstrated for Rh/MO$_x$ electrocatalysts.[350]

Along these lines, high-activity NbO₂-supported model electrocatalysts for the oxygen reduction reaction with ultralow (5 μg cm^{-2}) Pt content was demonstrated.[351] Pt/NbO₂/C electrocatalysts showed 3 times higher Pt mass activity for the ORR than those from a commercial Pt/C (with 10 μg cm^{-2} Pt loading) electrocatalyst. Similar enhancement is observed for the specific activity. The observed high activity of the Pt deposit was attributed to the reduced OH adsorption caused by lateral repulsion between PtOH and oxide surface species.

A promising approach to improve the durability and catalytic activity of non-carbon oxide supported Pt-based electrocatalysts is to combine TiO₂ with other oxides that are stable under oxidizing conditions; for example, ZrO₂, Ta₂O₅, RuO₂,[352] or showing proton or electron conductivity, for example, WO₃,[353,354] or MoO$_x$.[355] Ho et al.[355] prepared a Pt/Ti$_{0.7}$Mo$_{0.3}$O₂ model catalyst and demonstrated 7- and 2.6-fold higher ORR current densities of their oxide-supported catalyst compared with commercial Pt/C (ETEK) and PtCo/C (ETEK), respectively. Even the stability of the catalyst was quite high. Quite notably, Pt/Ti$_{0.7}$Mo$_{0.3}$O₂ showed no significant decrease in activity after 5000 cycles (potential cycling between 0 and 1.1 V at 50 mV s^{-1} in 0.5 M H₂SO₄ at 25 °C) and a performance loss of only 8% at 0.9 V. In sharp contrast, the activity of Pt/C showed a degradation of 50.6%,

and PtCo/C was reduced by 25.8%. They contributed the enhanced catalytic activity toward the ORR to the high electrical conductivity and specific catalytic reactivity of molybdenum oxide.[356]

For these new support materials, some co-catalytic activity was also shown, which could be explained by the SMSI between Pt particles and Ti$_x$Me$_y$O₂ (Me = transition metal) as well as enhanced inherent structural and chemical stability. For TiO₂-based support materials, it was shown by different groups that the ability to produce much thinner catalyst layers results in an increase in the current density at potentials lower than 0.7 V due to improved mass transport kinetics.[352,357]

Note that the aforementioned results concerning the durability and catalytic activity of the oxide-based electrocatalyst were generated mainly by ex situ experiments using, for example, a R(R)DE setup. Up to now, only a few results about durability and catalytic activity of oxide-supported Pt electrocatalysts exist. Huang et al.[357] performed in situ fuel cell measurements using a Pt/TiO₂ electrocatalyst with a Pt loading of 0.4 mg cm^{-2} at the cathode and 0.5 mg cm^{-2} at the anode side at 75 °C with fully humidified reactants. The electrochemical stability and performance of a Pt/TiO₂ electrocatalyst was examined using an accelerated stress test protocol suggested for PEFCs by the U.S. Department of Energy, which was slightly modified. The catalyst showed polarization curves, which were similar even after 200 h corrosion time (T_c) compared with a significant performance decrease of commercial Pt/C catalyst after T_c = 50 h. In addition, the group of Sasaki[331] performed in situ fuel cell experiments exploring the use of SnO₂ as a carbon-free support material for Pt electrocatalysts. They observed a relatively low electrochemical surface area (ECSA) and kinetic current densities for the ORR but satisfactory I−V curves compared with conventional Pt/C electrocatalysts. Really interesting is the high tolerance of their heat-treated SnO₂ against voltage cycling up to 1.3 V$_{RHE}$ displayed by a loss in ECSA from 14 to 10 m² g^{-1} after 10 000 cycles between 0.6 and 1.3 V at 80 °C, whereas Pt/C showed a decrease from 28 to nearly 0 m² g^{-1} after 4000 cycles.

All these investigations during recent years have shown that oxide support materials potentially offer higher stability under corroding fuel cell conditions compared with commercial carbon blacks and are usednot only to physically separate the catalyst nanoparticles and decrease their agglomeration rate. In addition, some studies demonstrate that the electronic nature of

the metal particles can be modified, thus positively affecting their chemisorption and catalytic properties. The significant enhancement of catalytic activity and durability by strong metal−support interactions as well as the achieved large surface areas make such systems very attractive for the application in DMFCs and PEFCs compared with commercial Pt electrocatalysts supported on carbon black materials.

Conductive Diamonds. A different and promising support material is represented by conductive diamonds (although carbon based), usually produced by doping diamonds with a secondary element, such as boron. They have been studied for about 2 decades due to their attractive properties as electrodes, such as high chemical stability in a broad potential window and low background currents.[358,359] Pure diamond is known as an insulator, but the conductivity can be improved by doping to increase the number of charge carriers and defects, but this can also have a negative effect (decrease) on the stability of the material. The electrical conductivity and, thus, the electrochemical behavior of doped diamond powders depend on different factors: (i) the concentration and the mobility of charge carriers, which depend on the nature and concentration of the dopant(s); (ii) the particle−particle connectivity; and (iii) nondiamond carbon impurities.

Wang and Swain developed a boron-doped diamond (BDD)-stabilized Pt catalyst, which showed no loss in activity, even after 2000 potential cycles between the hydrogen and oxygen evolution regime in 0.1 M HClO$_4$,[360] but poor interaction with the catalyst particles, low porosity, and high costs are still a limitation for its use as an alternative support material. The poor interaction between diamond support and catalyst particles can be enhanced by functionalization of the diamond surface with oxygen or hydrogen species. The presence of functional groups at the surface can have a strong influence on the metal particle size, morphology, stability and homogeneity of the dispersion.[361] In this work, a new approach based on highly crystalline insulating diamond particles (DP) acting as supports for Pd metal nanostructures was proposed. Despite the inherent bulk resistivity of DP, Pd centers appear interconnected to the electrode surface, possibly by hole-mediated surface transport characteristic of hydrogenated diamond surfaces.[362] They suggest that this surface conductivity in the Pd/DP composite is induced by partial hydrogenation of the diamond particle during the growth of the metal centers.

BDD is also considered a good substrate to study the intrinsic properties of deposited catalytic nanoparticles, avoiding the problems encountered with other common substrates (e.g., surface corrosion, oxide formation, or electronic interactions with catalyst particles). The very high stability of conductive BDD also allows study of the catalytic properties of precious metal oxide modifications from the level of submonolayers to a few monolayers, avoiding interactions with the generally adopted metal supports.[358]

5. FUTURE PERSPECTIVES AND CONCLUDING REMARKS

The development of fuel cell power plants and fuel cell systems for automotive applications has been gaining much more attention in the past 15 years; however, for the commercialization of these devices, a few remaining barriers need to be overcome: lower cost and proven durability. Around the world, industries are developing programs focused on improvement of the performance and durability of the fuel cell. Academia and industry reached major improvements in fuel cell activity in the

past 15 years, especially in the development of more active cathode materials. Although many other improvements in catalytic activity on the oxygen reduction reaction can be expected, the kinetic limitation seems still to pose a major obstacle.

The availability of a suitable fuel distribution and infrastructure is one of the factors that is strongly pushing research on direct alcohol fuel cells. As was summarized in this perspective, much effort is being placed on the development of catalysts for the complete oxidation of ethanol. Unfortunately, despite the fact of major improvements and beyond all the efforts, the effective oxidation of ethanol to CO$_2$ at reasonable potentials has not been achieved. As a summary, the most commonly used anode materials for DAFCs (methanol and ethanol) with superior performance are the binary and ternary alloys based on Pt−Ru and Pt−Sn catalysts. The larger catalytic activity toward alcohol oxidation results from the bifunctional effect (promoted mechanism) and the electronic interaction between Pt and alloyed metals (intrinsic mechanism). The C−C bond breaking remains the main problem in the ethanol oxidation reaction. To our knowledge, to attain the optimal performing DEFC, the catalyst development targets require a 2- to 3-fold enhancement of activity for ethanol oxidation. This target has not been achieved, and major efforts and further investments in this area need to be performed.

For both the anode and cathode sides of the PE fuel cell, the cost targets for automotive applications do not permit broad commercialization. Along these lines, two important approaches are being considered: improvement of the mass activity of precious metal catalysts by diminishing the metal loadings (without losing geometric activity) and the development of nonprecious metal catalysts.

Although the Pt and Pd alloys and core−shell systems show promising results toward the ORR, further improvements in activity are required, and durability of these systems still needs to be demonstrated in actual operating PEFC systems. It also should be noted that there seem to be some limits to improvements of the different Pt alloy catalysts. Although reports on, for instance, the absolute activities of different PtNi catalyst approaches appear to be differing sometimes by orders of magnitude because of different measurement and analysis conditions (for a discussion please refer to ref 363), the improvement factors versus the baseline Pt catalyst is always found in the range of 3−5.

The ORR on pyrolytic CoFe−C−N catalyst represents an interesting system free of precious metals with reduced cost. Transition metal −N−C heterocyclic catalysts have shown impressive activity and demonstrated lifetimes >1000 h; however, even with all the knowledge gained in the last 10 years, significant questions remain for these nonprecious metal catalysts: the identity of the active site and detailed mechanism, including the role of the transition metals and nitrogen in the catalysts. In addition, the activity of nonprecious metal catalysts is still far from the desirable activity and durability targets.

Along these lines, durability issues have attracted enormous attention in recent years. Despite the considerable understanding of electrocatalyst and catalyst layer degradation mechanisms and the different implemented mitigation strategies on the materials site, one of the main challenges in the immediate future is to develop new catalyst supports that improve the durability of the catalyst layer and, in a best-case scenario, also impact the electronic properties of the active phase to leapfrog to improved catalyst kinetics.

All the excellent improvements achieved since the early 2000s would not have been possible without the major developments in characterization methods and the contributions of the fundamental understanding of the materials, reaction mechanism and degradation of the catalyst layer achieved with the help from theoretical work. In terms of durability improvements, traditional Pt/C catalysts failed in 200−600 h of testing under load cycling conditions; however, the NSTF catalyst combined with the PFSA ionomer from 3M showed an increase in the MEA durability to beyond 7300 h. This achievement represents significant progress in MEA durability, and transferring these results into actual fuel cell system durability will definitively help to pave the way to commercialization .

Unquestionably, the main focus for the next decades will be the improvement of the PEFC lifetime and further cost reduction (which, by the way, is not only an electrocatalyst challenge, but also a challenge for materials and even important process engineering and production pathways). In this sense, it is expected that the development of novel functional materials, as catalyst and supports, will have great impact on the development of PEFCs in upcoming years.

■ AUTHOR INFORMATION

Corresponding Author
*E-mail: thomas.schmidt@phys.chem.ethz.ch.

Notes
The authors declare no competing financial interest.

■ ACKNOWLEDGMENTS

■ REFERENCES

(1) IPHE: International Partnership for Hydrogen and Fuel Cells in the Economy; *Fuel Cell Cost Analysis Summary*; http://www.iphe.net/docs/Resources/IPHE%20Fuel%20Cell%20Cost%20Comparison%20Report.pdf; 2009; Access date March 2012.

(2) Satyapal, S. Fuel Cell System Cost−2011; *DOE Hydrogen Program Record*; http://www.hydrogen.energy.gov/pdfs/11012_fuel_cell_system_cost.pdf; 2011; Access date March 2012.

(3) Debe, M. K. Advanced Cathode Catalysts and Supports for PEM Fuel Cells; *2011 Annual Merit Review DOE Hydrogen and Fuel Cells and Vehicle Technologies Programs*, 2011; Vol. *2012*.

(4) United States Council for Automotive Research; *Cell Component Accelerated Stress Test and Polarization Curve Protocols for Polymer Electrolyte Membrane Fuel Cells*; http://www.uscar.org/commands/files_download.php?files_id=267; 2012; Access date April 2012.

(5) Zelenay, P.; Chung, H.; Ding, Z.; Johnston, C. M.; Kim, Y. S.; Li, Q.; Trendewicz, A.; Turner, W.; Wu, G. *Advanced Materials and Concepts for Portable Power Fuel Cells*, 2011; http://www.hydrogen.energy.gov/pdfs/progress11/v_g_4_zelenay_2011.pdf.

(6) Yasuda, K.; Miyata, S. Durability Targets for Stationary and Automotive Applications in Japan. In *Polymer Electrolyte Fuel Cell Durability*; Büchi, F. N., Inaba, M., Schmidt, T. J., Eds.; Springer Science and Business Media LLC: New York, 2009; pp 489.

(7) U.S. Department of Energy. Hydrogen and Fuel Cells Program. In *Hydrogen and Fuel Cells Program*, 2012; Vol. *2012*.

(8) Roques, J.; Anderson, A. B. *J. Electrochem. Soc.* **2004**, *151*, E85.

(9) Anderson, A. B. *Phys. Chem. Chem. Phys.* **2011**, *14*, 1330.

(10) Norskov, J. K.; Rossmeisl, J.; Logadottir, A.; Lindqvist, L.; Kitchin, J. R.; Bligaard, T.; Jonsson, H. *J. Phys. Chem. B* **2004**, *108*, 17886.

(11) Norskov, J. K.; Bligaard, T.; Hvolbaek, B.; Abild-Pedersen, F.; Chorkendorff, I.; Christensen, C. H. *Chem. Soc. Rev.* **2008**, *37*, 2163.

(12) Rossmeisl, J.; Karlberg, G. S.; Jaramillo, T.; Norskov, J. K. *Faraday Discuss.* **2008**, *140*, 337.

(13) Greeley, J.; Stephens, I. E. L.; Bondarenko, A. S.; Johansson, T. P.; Hansen, H. A.; Jaramillo, T. F.; Rossmeisl, J.; Chorkendorff, I.; Norskov, J. K. *Nat. Chem.* **2009**, *1*, 552.

(14) Tritsaris, G. A.; Greeley, J.; Rossmeisl, J.; Norskov, J. K. *Catal. Lett.* **2011**, *141*, 909.

(15) Stephens, I. E. L.; Bondarenko, A. S.; Perez-Alonso, F. J.; Calle-Vallejo, F.; Bech, L.; Johansson, T. P.; Jepsen, A. K.; Frydendal, R.; Knudsen, B. P.; Rossmeisl, J.; Chorkendorff, I. *J. Am. Chem. Soc.* **2011**, *133*, 5485.

(16) Panchenko, A.; Koper, M. T. M.; Shubina, T. E.; Mitchell, S. J.; Roduner, E. *J. Electrochem. Soc.* **2004**, *151*, A2016.

(17) Hartnig, C.; Koper, M. T. M. *J. Electroanal. Chem.* **2002**, *532*, 165.

(18) Koper, M. T. M.; Vielstich, W.; Lamm, A.; Gasteiger, H. A. Numerical Simulations of Electrocatalytic Processes. In *Handbook of Fuel Cells. Fundamentals, Technology and Applications*; Vielstich, W., Lamm, A., Gasteiger, H. A., Eds.; John Wiley and Sons: Chichester, 2003; Vol. 2: Electrocatalysis; p 348.

(19) Schmidt, T. J.; Gasteiger, H. A.; Stäb, G. D.; Urban, P. M.; Kolb, D. M.; Behm, R. J. *J. Electrochem. Soc.* **1998**, *145*, 2354.

(20) Paulus, U. A.; Schmidt, T. J.; Gasteiger, H. A.; Behm, R. J. *J. Electroanal. Chem.* **2001**, *495*, 134.

(21) Schmidt, T. J.; Gasteiger, H. A.; Vielstich, W.; Gasteiger, H. A.; Lamm, A. Rotating Thin-Film Method for Supported Catalysts. In *Handbook of Fuel Cells: Fundamental, Technology, and Applications*; John Wiley & Sons: Chichester, 2003; Vol. 2: Electrocatalysis; p 316.

(22) Lucas, C. A.; Thompson, P.; Cormack, M.; Brownrigg, A.; Fowler, B.; Strmcnik, D.; Stamenkovic, V.; Greeley, J.; Menzel, A.; You, H.; Markovic, N. M. *J. Am. Chem. Soc.* **2009**, *131*, 7654.

(23) Stamenkovic, V. R.; Fowler, B.; Mun, B. S.; Wang, G.; Ross, P. N.; Lucas, C. A.; Markovic, N. M. *Science* **2007**, *315*, 493.

(24) Lucas, C. A.; Markovic, N. M.; Andrzej, W. In-Situ Surface X-ray Scattering and Infrared Reflection Adsorption Spectroscopy of CO Chemisorption at the Electrochemical Interface. In *In-situ Spectroscopic Studies of Adsorption at the Electrode and Electrocatalysis*; Sun, S.-G., Christensen, P. A., WieckowskiA., Eds.; Elsevier Science B.V.: Amsterdam, 2007; Chapter 11; p 339.

(25) Toney, M. F.; Koh, S.; Yu, C. F.; Strasser, P. Use of Anomalous X-ray Scattering for Probing the Structure, Composition and Size of Binary Alloy Nanoparticle Electrocatalysts. In *Proton Exchange Membrane Fuel Cells 8, Parts 1 and 2*, 2008; Vol. *16*; p 595.

(26) Yu, C. F.; Koh, S.; Leisch, J. E.; Toney, M. F.; Strasser, P. *Faraday Discuss.* **2008**, *140*, 283.

(27) Heinen, M.; Chen, Y. X.; Jusys, Z.; Behm, R. J. *Electrochim. Acta* **2007**, *53*, 1279.

(28) Osawa, M.; Komatsu, K.-i.; Samjeské, G.; Uchida, T.; Ikeshoji, T.; Cuesta, A.; Gutiérrez, C. *Angew. Chem., Int. Ed.* **2011**, *50*, 1159.

(29) Cuesta, A.; Cabello, G.; Gutierrez, C.; Osawa, M. *Phys. Chem. Chem. Phys.* **2011**, 13.

(30) Chen, Y. X.; Miki, A.; Ye, S.; Sakai, H.; Osawa, M. *J. Am. Chem. Soc.* **2003**, *125*, 3680.

(31) Chojak-Halseid, M.; Jusys, Z.; Behm, R. J. *J. Phys. Chem. C* **2010**, *114*, 22573.

(32) Halseid, M. C.; Jusys, Z.; Behm, R. J. *J. Electroanal. Chem.* **2010**, *644*, 103.

(33) Wang, H.; Löffler, T.; Baltruschat, H. *J. Appl. Electrochem.* **2001**, *31*, 759.

(34) Tuaev, X.; Strasser, P. Small Angle X-Ray Scattering (SAXS) Techniques for Polymer Electrolyte Fuel Cell Characterization. In *Polymer Electrolyte and Direct Methanol Fuel Cell Technology*; Hartnig, C., Roth, C., Eds.; Woodhead Publishing: Oxford, 2012; Vol. 2: In-situ Characterization techniques for low temperature fuel cells; pp 87−119.

(35) Liu, Z. Y.; Brady, B. K.; Carter, R. N.; Litteer, B.; Budinski, M.; Hyun, J. K.; Muller, D. A. *J. Electrochem. Soc.* **2008**, *155*, B979.

(36) Xin, H. L.; Mundy, J. A.; Liu, Z.; Cabezas, R.; Hovden, R.; Kourkoutis, L. F.; Zhang, J.; Subramanian, N. P.; Makharia, R.; Wagner, F. T.; Muller, D. A. *Nano Lett.* **2011**, *12*, 490.

(37) Mayrhofer, K. J. J.; Ashton, S. J.; Meier, J. C.; Wiberg, G. K. H.; Hanzlik, M.; Arenz, M. *J. Power Sources* **2008**, *185*, 734.

(38) Wang, C.; van der Vilet, D.; Chang, K.-C.; You, H.; Strmcnik, D.; Schlueter, J. A.; Markovic, N. M.; Stamenkovic, V. R. *J. Phys. Chem. C* **2009**, *113*, 19365.

(39) Wang, C.; Chi, M.; Wang, G.; van der Vliet, D.; Li, D.; More, K.; Wang, H.-H.; Schlueter, J. A.; Markovic, N. M.; Stamenkovic, V. R. *Adv. Funct. Mater.* **2011**, *21*, 147.

(40) Somorjai, G. A.; Park, J. Y. *Top.Catal.* **2008**, *49*, 126.

(41) Habas, S. E.; Lee, H.; Radmilovic, V.; Somorjai, G. A.; Yang, P. *Nat. Mater.* **2007**, *6*, 692.

(42) Chen, Q. S.; Vidal-Iglesias, F. J.; Solla-Gullon, J.; Sun, S. G.; Feliu, J. M. *Chem. Sci.* **2012**, *3*, 136.

(43) Inaba, M.; Ando, M.; Hatanaka, A.; Nomoto, A.; Matsuzawa, K.; Tasaka, A.; Kinumoto, T.; Iriyama, Y.; Ogumi, Z. *Electrochim. Acta* **2006**, *52*, 1632.

(44) Chrzanowski, W.; Wieckowski, A. *Langmuir* **1998**, *14*, 1967.

(45) Tremiliosi-Filho, G.; Kim, H.; Chrzanowski, W.; Wieckowski, A.; Grzybowska, B.; Kulesza, P. *J. Electroanal. Chem.* **1999**, *467*, 143.

(46) Beden, B.; Kadirgan, F.; Lamy, C.; Leger, J. M. *J. Electroanal. Chem. Interfacial Electrochem.* **1981**, *127*, 75.

(47) Kabbabi, A.; Faure, R.; Durand, R.; Beden, B.; Hahn, F.; Leger, J. M.; Lamy, C. *J. Electroanal. Chem.* **1998**, *444*, 41.

(48) Lima, A.; Coutanceau, C.; Leger, J. M.; Lamy, C. *J. Appl. Electrochem.* **2001**, *31*, 379.

(49) Dubau, L.; Hahn, F.; Coutanceau, C.; Leger, J. M.; Lamy, C. *J. Electroanal. Chem.* **2003**, *554*, 407.

(50) Grozovski, V.; Climent, V.; Herrero, E.; Feliu, J. M. *J. Electroanal. Chem.* **2011**, *662*, 43.

(51) Wang, H.; Rus, E.; Abruña, H. D. *Anal. Chem.* **2010**, *82*, 4319.

(52) Binder, H.; Köhling, A.; Sandstede, G. Effect of Alloying Components on the Catalytic Activity of Platinum in the Case of Carbonaceous Fuels. In *From Electrocotalysis to Fuel Cells*; Sanstede, G., Eds.; Battelle Seattle Research Center by the University of Washington Press: Seattle, London, 1972.

(53) Gasteiger, H. A.; Markovic, N.; Ross, P. N.; Cairns, E. J. *J. Phys. Chem.* **1993**, *97*, 12020.

(54) Gasteiger, H. A.; Markovic, N.; Ross, P. N.; Cairns, E. J. *Electrochim. Acta* **1994**, *39*, 1825.

(55) Gasteiger, H. A.; Markovic, N.; Ross, P. N.; Cairns, E. J. *J. Electrochem. Soc.* **1994**, *141*, 1795.

(56) Markovic, N. M.; Ross, P. N., Jr *Surf. Sci. Rep.* **2002**, *45*, 117.

(57) Parsons, R.; VanderNoot, T. *J. Electroanal. Chem. Interfacial Electrochem.* **1988**, *257*, 9.

(58) Lai, S.; Lebedeva, N.; Housmans, T.; Koper, M. *Top. Catal.* **2007**, *46*, 320.

(59) Watanabe, M.; Motoo, S. *J. Electroanal. Chem. Interfacial Electrochem.* **1975**, *60*, 275.

(60) Lebedeva, N. P.; Rodes, A.; Feliu, J. M.; Koper, M. T. M.; van Santen, R. A. *J. Phys. Chem. B* **2002**, *106*, 9863.

(61) Lebedeva, N. P.; Koper, M. T. M.; Feliu, J. M.; van Santen, R. A. *J. Phys. Chem. B* **2002**, *106*, 12938.

(62) Yan, Y.-G.; Yang, Y.-Y.; Peng, B.; Malkhandi, S.; Bund, A.; Stimming, U.; Cai, W.-B. *J. Phys. Chem. C* **2011**, *115*, 16378.

(63) Arenz, M.; Stamenkovic, V.; Schmidt, T. J.; Wandelt, K.; Ross, P. N.; Markovic, N. M. *Phys. Chem. Chem. Phys.* **2003**, *5*.

(64) Climent, V. Ì. c.; Herrero, E.; Feliu, J. M. *Electrochim. Acta* **1998**, *44*, 1403.

(65) Macia, M. D.; Herrero, E.; Feliu, J. M. *Electrochim. Acta* **2002**, *47*, 3653.

(66) Yajima, T.; Uchida, H.; Watanabe, M. *J. Phys. Chem. B* **2004**, *108*, 2654.

(67) Pereira, M. G.; Jimenez, M. D.; Elizalde, M. P.; Manzo-Robledo, A.; Alonso-Vante, N. *Electrochim. Acta* **2004**, *49*, 3917.

(68) Lai, S. C. S.; Koper, M. T. M. *J. Phys. Chem. Lett.* **2010**, *1*, 1122.

(69) Lai, S. C. S.; Kleyn, S. E. F.; Rosca, V.; Koper, M. T. M. *J. Phys. Chem. C* **2008**, *112*, 19080.

(70) Colmati, F.; Tremiliosi-Filho, G.; Gonzalez, E. R.; Berna, A.; Herrero, E.; Feliu, J. M. *Phys. Chem. Chem. Phys.* **2009**, *11*, 9114.

(71) Kwon, Y.; Schouten, K. J. P.; Koper, M. T. M. *ChemCatChem* **2011**, *3*, 1176.

(72) Kerangueven, G.; Coutanceau, C.; Sibert, E.; Leger, J. M.; Lamy, C. *J. Power Sources* **2006**, *157*, 318.

(73) Coutanceau, C.; Kerangueven, G.; Sibert, E.; Leger, J. M.; Lamy, C. *J. Power Sources* **2006**, *157*.

(74) Lamy, C.; Belgsir, E. M.; Leger, J. M. *J. Appl. Electrochem.* **2001**, *31*, 799.

(75) Leger, J. M.; Rousseau, S.; Coutanceau, C.; Hahn, F.; Lamy, C. *Electrochim. Acta* **2005**, *50*, 5118.

(76) Vigier, F.; Coutanceau, C.; Perrard, A.; Belgsir, E. M.; Lamy, C. *J. Appl. Electrochem.* **2004**, *34*, 439.

(77) Tremiliosi-Filho, G.; Gonzalez, E. R.; Motheo, A. J.; Belgsir, E. M.; Leger, J. M.; Lamy, C. *J. Electroanal. Chem.* **1998**, *444*, 31.

(78) Lai, S. C. S.; Kleyn, S. E. F.; Rosca, V.; Koper, M. T. M. *J. Phys. Chem. C* **2008**, *112*, 19080.

(79) Vigier, F.; Coutanceau, C.; Hahn, F.; Belgsir, E. M.; Lamy, C. *J. Electroanal. Chem.* **2004**, *563*, 81.

(80) Shao, M. H.; Adzic, R. R. *Electrochim. Acta* **2005**, *50*, 2415.

(81) Del Colle, V.; Souza-Garcia, J.; Tremiliosi-Filho, G.; Herrero, E.; Feliu, J. M. *Phys. Chem. Chem. Phys.* **2011**, *13*, 12163.

(82) Souza-Garcia, J.; Herrero, E.; Feliu, J. M. *ChemPhysChem* **2010**, *11*, 1391.

(83) Colmati, F.; Tremiliosi-Filho, G.; Gonzalez, E. R.; Berna, A.; Herrero, E.; Feliu, J. M. *Faraday Discuss.* **2008**, *140*, 379.

(84) Lai, S. C. S.; Koper, M. T. M. *Faraday Discuss.* **2008**, *140*, 399.

(85) Zhou, Z.-Y.; Huang, Z.-Z.; Chen, D.-J.; Wang, Q.; Tian, N.; Sun, S.-G. *Angew. Chem., Int. Ed.* **2009**, *49*, 411.

(86) Tian, N.; Zhou, Z.-Y.; Sun, S.-G. *J. Phys. Chem. C* **2008**, *112*, 19801.

(87) Na, T.; Zhi-You, Z.; Shi-Gang, S.; Yong, D.; Zhong Lin, W. *Science* **2007**, *316*.

(88) Zhou, W.-P.; Li, M.; Koenigsmann, C.; Ma, C.; Wong, S. S.; Adzic, R. R. *Electrochim. Acta* **2011**, *56*, 9824.

(89) Koenigsmann, C.; Zhou, W.-p.; Adzic, R. R.; Sutter, E.; Wong, S. S. *Nano Letters* **2010**, *10*, 2806.

(90) Camara, G. A.; de Lima, R. B.; Iwasita, T. *Electrochem. Commun.* **2004**, *6*, 812.

(91) Rousseau, S.; Coutanceau, C.; Lamy, C.; Leger, J. M. *J. Power Sources* **2006**, *158*, 18.

(92) Giz, M. J.; Camara, G. A.; Maia, G. *Electrochem. Commun.* **2009**, *11*, 1586.

(93) Lima, F. H. B.; Gonzalez, E. R. *Electrochim. Acta* **2008**, *53*, 2963.

(94) Fujiwara, N.; Friedrich, K. A.; Stimming, U. *J. Electroanal. Chem.* **1999**, *472*, 120.

(95) Zhou, W.-P.; Axnanda, S.; White, M. G.; Adzic, R. R.; Hrbek, J. *J. Phys. Chem. C* **2011**, *115*, 16467.

(96) Purgato, F. L. S.; Olivi, P.; Leger, J. M.; de Andrade, A. R.; Tremiliosi-Filho, G.; Gonzalez, E. R.; Lamy, C.; Kokoh, K. B. *J. Electroanal. Chem.* **2009**, *628*, 81.

(97) Neto, A. O.; Giz, M. J.; Perez, J.; Ticianelli, E. A.; Gonzalez, E. R. *J. Electrochem. Soc.* **2002**, *149*, A272.

(98) de Souza, J. P. I; Queiroz, S. L.; Bergamaski, K.; Gonzalez, E. R.; Nart, F. C. *J. Phys. Chem. B* **2002**, *106*, 9825.

(99) Spinace, E. V.; Neto, A. O.; Vasconcelos, T. R. R.; Linardi, M. *J. Power Sources* **2004**, *137*, 17.

(100) Lamy, C.; Rousseau, S.; Belgsir, E. M.; Coutanceau, C.; Leger, J. M. *Electrochim. Acta* **2004**, *49*, 3901.

(101) Zhou, W. J.; Song, S. Q.; Li, W. Z.; Zhou, Z. H.; Sun, G. Q.; Xin, Q.; Douvartzides, S.; Tsiakaras, P. *J. Power Sources* **2005**, *140*, 50.

(102) Colmati, F.; Antolini, E.; Gonzalez, E. R. *J. Power Sources* **2006**, *157*, 98.

(103) Wang, H.; Jusys, Z.; Behm, R. J. *J. Power Sources* **2006**, *154*, 351.

(104) Chu, Y. H.; Shul, Y. G. *Int. J. Hydrogen Energy* **2010**, *35*, 11261.

(105) Li, M.; Kowal, A.; Sasaki, K.; Marinkovic, N.; Su, D.; Korach, E.; Liu, P.; Adzic, R. R. *Electrochim. Acta* **2010**, *55*, 4331.

(106) Jian, X.-H.; Tsai, D.-S.; Chung, W.-H.; Huang, Y.-S.; Liu, F.-J. *J. Mater. Chem.* **2009**, *19*, 1601.

(107) Garcia, G.; Tsiouvaras, N.; Pastor, E.; Peña, M. A.; Fierro, J. L. G.; Martinez-Huerta, M. V. *Int. J. Hydrogen Energy* **2012**, *37*, 7131−7140

(108) Wang, Z.-B.; Yin, G.-P.; Lin, Y.-G. *J. Power Sources* **2007**, *170*, 242.

(109) Lee, E.; Murthy, A.; Manthiram, A. *Electrochim. Acta* **2010**, *56*, 1611.

(110) Kowal, A.; Li, M.; Shao, M.; Sasaki, K.; Vukmirovic, M. B.; Zhang, J.; Marinkovic, N. S.; Liu, P.; Frenkel, A. I.; Adzic, R. R. *Nat. Mater.* **2009**, *8*, 325.

(111) Markovic, N. M.; Schmidt, T. J.; Stamenkovic, V.; Ross, P. N. *Fuel Cells* **2001**, *1*, 105.

(112) Tripkovic, V.; Skulason, E.; Siahrostami, S.; Norskov, J. K.; Rossmeisl, J. *Electrochim. Acta* **2010**, *55*, 7975.

(113) Markovic, N. M.; Gasteiger, H. A.; Ross, P. N. *J. Phys. Chem.* **1995**, *99*, 3411.

(114) Markovic, N. M.; Gasteiger, H. A.; Ross, P. N. *J. Electrochem. Soc.* **1997**, *144*, 1591.

(115) Markovic, N. M.; Gasteiger, H. A.; Ross, P. N. *J. Phys. Chem.* **1996**, *100*, 6715.

(116) Schmidt, T. J.; Stamenkovic, V.; Ross, P. N., Jr.; Markovic, N. M. *Phys. Chem. Chem. Phys.* **2003**, *5*, 400.

(117) Kuzume, A.; Herrero, E.; Feliu, J. M. *J. Electroanal. Chem.* **2007**, *599*, 333.

(118) Sanchez-Sanchez, C. M.; Solla-Gullon, J.; Vidal-Iglesias, F. J.; Aldaz, A.; Montiel, V.; Herrero, E. *J. Am. Chem. Soc.* **2010**, *132*, 5622.

(119) Luczak, F. J.; Landsman, D. A. In *Handbook of Fuel Cells-Fundamentals: Technology and Applications*; Vielstich, W., Lamm, A., Gasteiger, H. A., Eds.; Wiley-VCH: Chichester, 2003; pp 811.

(120) Jalan, V.; Taylor, E. J. *J. Electrochem. Soc.* **1983**, *130*, 2299.

(121) Mukerjee, S.; Srinivasan, S. *J. Electroanal. Chem.* **1993**, *357*, 201.

(122) Toda, T.; Igarashi, H.; Watanabe, M. *J. Electrochem. Soc.* **1998**, *145*, 4185.

(123) Toda, T.; Igarashi, H.; Watanabe, M. *J. Electroanal. Chem.* **1999**, *460*, 258.

(124) Toda, T.; Igarashi, H.; Uchida, H.; Watanabe, M. *J. Electrochem. Soc.* **1999**, *146*, 3750.

(125) Gasteiger, H. A.; Kocha, S. S.; Sompalli, B.; Wagner, F. T. *Appl. Catal., B* **2005**, *56*, 9.

(126) Mukerjee, S.; Srinivasan, S.; Soriaga, M. P.; McBreen, J. *J. Electrochem. Soc.* **1995**, *142*, 1409.

(127) Mukerjee, S.; Srinivasan, S.; Vielstich, W.; Gasteiger, H. A.; Lamm, A. O₂ Reduction and Structure-Related Parameters for Supported Catalysts. In *Handbook of Fuel Cells−Fundamentals, Technology and Applications; Vol. 2: Electrocatalysis*; Vielstich, W., Gasteiger, H. A., Lamm, A., Eds.; John Wiley & Sons: Chichester, 2003; Vol. 2; pp 502.

(128) Wang, C.; Chi, M.; Li, D.; van der Vliet, D.; Wang, G.; Lin, Q.; Mitchell, J. F.; More, K. L.; Markovic, N. M.; Stamenkovic, V. R. *ACS Catal.* **2011**, *1*, 1355.

(129) Wang, C.; Wang, G.; van der Vliet, D.; Chang, K.-C.; Markovic, N. M.; Stamenkovic, V. R. *Phys. Chem. Chem. Phys.* **2010**, *12*, 6933.

(130) Yang, H.; Vogel, W.; Lamy, C.; Alonso-Vante, N. *J. Phys. Chem. B* **2004**, *108*, 11024.

(131) Paulus, U. A.; Wokaun, A.; Scherer, G. G.; Schmidt, T. J.; Stamenkovic, V.; Radmilovic, V.; Markovic, N. M.; Ross, P. N. *J. Phys. Chem. B* **2002**, *106*, 4181.

(132) Huang, Q.; Yang, H.; Tang, Y.; Lu, T.; Akins, D. L. *Electrochem. Commun.* **2006**, *8*, 1220.

(133) Paulus, U. A.; Scherer, G. G.; Wokaun, A.; Schmidt, T. J.; Stamenkovic, V.; Markovic, N. M.; Ross, P. N., Jr. *Electrochim. Acta* **2002**, *47*, 3787.

(134) Polak, M.; Rubinovich, L. *Surf. Sci. Rep.* **2000**, *38*, 127.

(135) Wang, C.; Chi, M.; Li, D.; Strmcnik, D.; van der Vliett, D.; Wang, G.; Komanicky, V.; Chang, K.-C.; Paulikas, A. P.; Tripkovic, D.; Pearson, J.; More, K. L.; Markovic, N. M.; Stamenkovic, V. R. *J. Am. Chem. Soc.* **2011**, *133*, 14396.

(136) Stamenkovic, V.; Schmidt, T. J.; Ross, P. N.; Markovic, N. M. *J. Phys. Chem. B* **2002**, *106*, 11970.

(137) Stamenkovic, V.; Schmidt, T. J.; Markovic, N. M.; Ross, P. N., Jr. *J. Electroanal. Chem.* **2003**, *554−555*, 191.

(138) Stamenkovic, V.; Mun, B. S.; Mayrhofer, K. J. J.; Ross, P. N.; Markovic, N. M.; Rossmeisl, J.; Greeley, J.; Norskov, J. K. *Angew. Chem., Int. Ed.* **2006**, *45*, 2897.

(139) Stamenkovic, V. R.; Mun, B. S.; Arenz, M.; Mayrhofer, K. J. J.; Lucas, C. A.; Wang, G.; Ross, P. N.; Markovic, N. M. *Nat. Mater.* **2007**, *6*, 241.

(140) Greeley, J.; Noskov, J. K.; Mavrikakis, M. *Annu. Rev. Phys. Chem.* **2002**, *53*, 319.

(141) Hammer, B.; Morikawa, Y.; Noskov, J. K. *Phys. Rev. Lett.* **1996**, *76*, 2141.

(142) Zhang, J.; Yang, H.; Fang, J.; Zou, S. *Nano Lett.* **2010**, *10*, 638.

(143) Wang, C.; van der Vliet, D.; More, K. L.; Zaluzec, N. J.; Peng, S.; Sun, S.; Daimon, H.; Wang, G.; Greeley, J.; Pearson, J.; Paulikas, A. P.; Karapetrov, G.; Strmcnik, D.; Markovic, N. M.; Stamenkovic, V. R. *Nano Lett.* **2010**, *11*, 919.

(144) Oezaslan, M.; Strasser, P. *J. Power Sources* **2010**, *196*, 5240.

(145) Strasser, P.; Koh, S.; Anniyev, T.; Greeley, J.; More, K.; Yu, C.; Liu, Z.; Kaya, S.; Nordlund, D.; Ogasawara, H.; Toney, M. F.; Nilsson, A. *Nat. Chem.* **2010**, *2*, 454.

(146) Mani, P.; Srivastava, R.; Strasser, P. *J. Phys. Chem. C* **2008**, *112*, 2770.

(147) Strasser, P.; Koha, S.; Greeley, J. *Phys. Chem. Chem. Phys.* **2008**, *10*, 3670.

(148) Koh, S.; Strasser, P. *J. Am. Chem. Soc.* **2007**, *129*, 12624.

(149) Hasche, F.; Oezaslan, M.; Strasser, P. *Chemcatchem* **2011**, *3*, 1805.

(150) Mani, P.; Srivastava, R.; Strasser, P. *J. Power Sources* **2011**, *196*, 666.

(151) Hasche, F.; Oezaslan, M.; Strasser, P. *J. Electrochem. Soc.* **2012**, *159*, B25.

(152) Zhang, J.; Sasaki, K.; Sutter, E.; Adzic, R. R. *Science* **2007**, *315*, 220.

(153) Lim, B.; Jiang, M.; Camargo, P. H. C.; Cho, E. C.; Tao, J.; Lu, X.; Zhu, Y.; Xia, Y. *Science* **2009**, *324*, 1302.

(154) Rodríguez, P.; Koverga, A. A.; Koper, M. T. M. *Angew. Chem., Int. Ed.* **2010**, *49*, 1241.

(155) Rodriguez, P.; Kwon, Y.; Koper, M. T. M. *Nat. Chem.* **2012**, *4*, 177.

(156) Rodriguez, P.; Garcia-Araez, N.; Koper, M. T. M. *Phys. Chem. Chem. Phys.* **2010**, *12*, 9373.

(157) Escudero-Escribano, M.; Zoloff Michoff, M. E.; Leiva, E. P. M; Markovic, N. M.; Gutierrez, C.; Cuesta, A. *ChemPhysChem* **2011**, *12*, 2230.

(158) Strmcnik, D.; Escudero-Escribano, M.; Kodama, K.; Stamenkovic, V. R.; Cuesta, A.; Markovic, N. M. *Nat. Chem.* **2010**, *2*, 880.

(159) Genorio, B.; Strmcnik, D.; Subbaraman, R.; Tripkovic, D.; Karapetrov, G.; Stamenkovic, V. R.; Pejovnik, S.; Markovic, N. M. *Nat. Mater.* **2010**, *9*, 998.

(160) Snyder, J.; Fujita, T.; Chen, M. W.; Erlebacher, J. *Nat. Mater.* **2010**, *9*, 904.

(161) Steel, D. C.; Benicewicz, B. C.; Xiao, L.; Schmidt, T. J. High-Temperature Polybenzimidazole-Based Membranes. In *Handbook of Fuel Cells−Fundamentals, Technology and Applications*; Vielstich, W., Yokokawa, H., Gasteiger, H. A., Eds.; John Wiley & Sons: New York, 2009; pp 300.

(162) Buechi, F. N.; Inaba, M.; Schmidt, T. J.; Buechi, F. N.; Inaba, M.; Schmidt, T. J. *Polymer Electrolyte Fuel Cell Durability*; Springer: New Vork, 2009.

(163) *Handbook of Fuel Cells−Advances in Electrocatalysis, Materials, Diagnostics and Durability*; Vielstich, W., Gasteiger, H. A., Yokokawa, H., Eds.; Wiley-VCH: Chichester, 2009, Vol. *5, 6.*

(164) *Polymer Electrolyte Fuel Cells 10−ECS Transactions*; Gasteiger, H. A., Uchida, H., Ramani, V., Weber, A., Schmidt, T. J., Fuller, T. F., Strasser, P., Shirvanian, P., Inaba, M., Edmundson, M., Buechi, F. N., Jones, D. J., Lamy, C., Mantz, R., Narayanan, S., Darling, R. M., Zawodzinski, T., Eds.; The Electrochemical Society: Pennington, NJ, 2010; Vol. *33*; issue 1.

(165) *Polymer Electrolyte Fuel Cells 11−ECS Transactions*; Gasteiger, H. A., Buechi, F. N., Ramani, V., Weber, A., Shirvanian, P., Fuller, T. F., Narayanan, S., Nakagawa, H., Edmundson, M., Jones, D. J., Uchida, H., Lamy, C., Strasser, P., Mukerjee, S., Mantz, R., Swider-Lyons, K., Schmidt, T. J., Eds.; The Electrochemical Society: Pennington, NJ, 2011, Vol. *41*, issue 1.

(166) Kinoshita, K. *Carbon. Electrochemical and Physicochemical Properties*; John Wiley & Sons: New York, 1988.

(167) Wagner, F. T.; Yan, S. G.; Yu, P. T. Catalyst and Catalyst-Support Durability. In *Handbook of Fuel Cells−Fundamentals, Technology and Applications*; Vielstich, W., Yokokawa, H., Gasteiger, H. A., Eds.; John Wiley & Sons: Chichester, 2009; Vol. *5*: Advances in Electrocatalysis, Materials, Diagnostics and Durability; p 250.

(168) Yu, P. T.; Gu, W.; Zhang, J.; Makharia, M.; Wagner, F. T.; Gasteiger, H. A. Carbon Support Requirements for Highly Durable Fuel Cell Operation. In *Polymer Electrolyte Fuel Cell Durability*; Büchi, F. N., Inaba, M., Schmidt, T. J., Eds.; Springer Science and Bussiness Media: New York, 2009; p 29.

(169) Mathias, M. F.; Makharia, R.; Gasteiger, H. A.; Conley, J. J.; Fuller, T. J.; Gittleman, C. J.; Kocha, S. S.; Miller, D. P.; Mittelstaedt, C. K.; Xie, T.; Yan, S. G.; Yu, P. T. *Electrochem. Soc. Interface* 2005, *14*, 24.

(170) Reiser, C. A.; Bregoli, L. J.; Patterson, T. W.; Yi, J. S.; Yang, J. D.; Perry, M. L.; Jarvi, T. D. *Electrochem. Solid-State Lett.* 2005, *8*, A273.

(171) Tang, H.; Qi, Z. G.; Ramani, M.; Elter, J. F. *J. Power Sources* 2006, *158*, 1306.

(172) Schmidt, T. J. High Temperature Polymer Electrolyte Fuel Cells: Durability Insights. In *Polymer Electrolyte Fuel Cell Durability*; Buechi, F. N., Inaba, M., Schmidt, T. J., Eds.; Springer: New York, 2009; p 199.

(173) Markovic, N. M.; Schmidt, T. J.; Grgur, B. N.; Gasteiger, H. A.; Ross, P. N., Jr.; Behm, R. J. *J. Phys. Chem. B* 1999, *103*, 8568.

(174) Tang, L.; Han, B.; Persson, K.; Friesen, C.; He, T.; Sieradziki, K.; Ceder, G. *J. Am. Chem. Soc.* 2010, *132*, 596.

(175) Pourbaix, M. *Atlas of Electrochemical Equilibria in Aqueous Solutions*; National Association of Corrosion Engineers: Houston, TX, 1974.

(176) Gu, W.; Yu, P. T.; Carter, R. N.; Makharia, M.; Gasteiger, H. A. Modeling of Membrane-Electrode-Assembly Degradation in Proton-Exchange-Membrane Fuel Cells: Local H$_2$ Starvation and Start−Stop Induced Carbon Support Corrosion. In *Modeling and Diagnostics of Polymer Electrolyte Fuel Cells*; Pasaogullari, C.-Y. W., Ed.; Springer Science + Business Media, LLC: New York, 2010; Vol. *49*; p 45.

(177) Perry, M. L.; Darling, R. M.; Kandoi, S.; Patterson, T. W.; Reiser, C. A. Operating Requirements for Durable Polymer-Electrolyte Fuel Cell Stacks. In *Polymer Electrolyte Fuel Cell Durability*; Büchi, F. N., Inaba, M., Schmidt, T. J., Eds.; Springer Science + Business LLC: New York, 2009; p 399.

(178) Perry, M. L.; Patterson, T. W.; Reiser, C. A. *ECS Trans.* 2006, *3*, 783.

(179) Hartnig, C.; Schmidt, T. J. *J. Power Sources* 2011, *196*, 5564.

(180) Schulenburg, H.; Schwanitz, B.; Linse, N.; Scherer, G. G.; Wokaun, A.; Krbanjevic, J.; Grothausmann, R.; Manke, I. *J. Phys. Chem. C* 2011, *115*, 14236.

(181) Bett, J. A. S.; Cipollini, N. E.; Jarvi, T. D.; Breault, R. D. *UTC Fuel Cells.* US Patent 6,855,453, 2005.

(182) Ralph, T. R.; Hudson, S.; Wilkinson, D. P. *ECS Trans.* 2006, *1*, 67.

(183) Genorio, B.; Strmcnik, D.; Subbaraman, R.; Tripkovic, D.; Karapetrov, G.; Stamenkovic, V. R.; Pejovnik, S.; Markovic, N. M. *Nat. Mater.* 2010, *9*, 998.

(184) Schmidt, T. J.; Baurmeister, J. *J. Power Sources* 2008, *176*, 428.

(185) Lamy, C.; Jones, D. J.; Coutanceau, C.; Brault, P.; Martemianov, S.; Bultel, Y. *Electrochim. Acta* 2011, *56*, 10406.

(186) Schwanitz, B.; Schulenburg, H.; Horisberger, M.; Wokaun, A.; Scherer, G. G. *Electrocatalysis* 2011, *2*, 35.

(187) Schwanitz, B.; Rabis, A.; Horisberger, M.; Scherer, G. G.; Schmidt, T. J. *Chimia* 2012, *66*, 110−119.

(188) Debe, M. K.; Schmoeckel, A. K.; Vernstrorn, G. D.; Atanasoski, R. *J. Power Sources* 2006, *161*, 1002.

(189) Patterson, T. W. In *Fuel Cell Technology Topical Conference Proceedings*; Igwe, G. J., Mah, D., Eds.; AIChE Spring National Meeting, New York, AIChE: New York, 2002; p 313.

(190) Ferreira, P. J.; la O, G. J.; Shao-Horn, Y.; Morgan, D.; Makharia, R.; Kocha, S.; Gasteiger, H. A. *J. Electrochem. Soc.* 2005, *152*, A2256.

(191) Schulenburg, H.; Schwanitz, B.; Krbanjevic, J.; Linse, N.; Scherer, G. n. G.; Wokaun, A. *Electrochem. Commun.* 2011, *13*, 921.

(192) Sasaki, K.; Shao, M.; Adzic, R. R. Dissolution and Stabilization of Platinum in Oxygen Cathodes. In *Polymer Electrolyte Fuel Cell Durability*; Büchi, F. N., Inaba, M., Schmidt, T. J., Eds.; Springer Science + Business Media, LLC: New York, 2009; p 7.

(193) Sasaki, K.; Naohara, H.; Cai, Y.; Choi, Y. M.; Liu, P.; Vukmirovic, M. B.; Wang, J. X.; Adzic, R. R. *Angew. Chem., Int. Ed.* 2010, *49*, 8602.

(194) Sasaki, K.; Wang, J. X.; Naohara, H.; Marinkovic, N.; More, K.; Inada, H.; Adzic, R. R. *Electrochim. Acta* 2010, *55*, 2645.

(195) Wang, J. X.; Ma, C.; Choi, Y. M.; Su, D.; Zhu, Y. M.; Liu, P.; Si, R.; Vukmirovic, M. B.; Zhang, Y.; Adzic, R. R. *J. Am. Chem. Soc.* 2011, *133*, 13551.

(196) Debe, M. K.; Poirier, R. J. *J. Vacuum Sci. Technol., A* 1994, *12*, 2017.

(197) Debe, M. K.; Drube, A. R. *J. Vac. Sci. Technol., B: Nanotechnol. Microelectron.: Mater., Process., Meas., Phenom.* 1995, *13*, 1236.

(198) Debe, M. K. Novel catalyst, catalyst support and catalyst coated membrane methods. In *Handbook of Fuel Cells—Fundamentals, Technology and Applications*; Vielstich, W.; Lamb, A., Gasteiger, H. A., Eds.; John Wiley & Sons, 2003; Vol. *3*; p 677.

(199) Stahl, J. B.; Debe, M. K.; Coleman, P. L. *J. Vac. Sci. Technol., A* 1996, *14*, 1761.

(200) Debe, M. K.; Steinbach, A. J.; Vernstrom, G. D.; Hendricks, S. M.; Kurkowski, M. J.; Atanasoski, R. T.; Kadera, P.; Stevens, D. A.; Sanderson, R. J.; Marvel, E.; Dahn, J. R. *J. Electrochem. Soc.* 2011, *158*, B910.

(201) van der Vliet, D.; Wang, C.; Debe, M.; Atanasoski, R.; Markovic, N. M.; Stamenkovic, V. R. *Electrochim. Acta* 2011, *56*, 8695.

(202) Gancs, L.; Kobayashi, T.; Debe, M. K.; Atanasoski, R.; Wieckowski, A. *Chem. Mater.* 2008, *20*, 2444.

(203) Paulus, U. A.; Veziridis, Z.; Schnyder, B.; Kuhnke, M.; Scherer, G. G.; Wokaun, A. *J. Electroanal. Chem.* 2003, *541*, 77.

(204) Liu, G. C.-K.; Stevens, D. A.; Burns, J. C.; Sanderson, R. J.; Vernstrom, G.; Atanasoski, R. T.; Debe, M. K.; Dahn, J. R. *J. Electrochem. Soc.* 2011, *158*, B919.

(205) Bonakdarpour, A.; Stevens, K.; Vernstrom, G. D.; Atanasoski, R.; Schmoeckel, A. K.; Debe, M. K.; Dahn, J. R. *Electrochim. Acta* 2007, *53*, 688.

(206) Nesselberger, M.; Ashton, S.; Meier, J. C.; Katsounaros, I.; Mayrhofer, K. J. J.; Arenz, M. *J. Am. Chem. Soc.* 2011, *133*, 17428.

(207) Mayrhofer, K. J. J.; Blizanac, B. B.; Arenz, M.; Stamenkovic, V.; Ross, P. N.; Markovic, N. M. *J. Phys. Chem. B* 2005, *109*, 14433.

(208) Debe, M. K.; Steinbach, A. J.; Vernstrom, G. D.; Hendricks, S. M.; Kurkowski, M. J.; Atanasoski, R. T.; Kadera, P.; Stevens, D. A.; Sanderson, R. J.; Marvel, E.; Dahn, J. R. *J. Electrochem. Soc.* 2011, *158*, B910.

(209) Garsuch, A.; Stevens, D. A.; Sanderson, R. J.; Wang, S.; Atanasoski, R. T.; Hendricks, S.; Debe, M. K.; Dahn, J. R. *J. Electrochem. Soc.* 2010, *157*, B187.

(210) Liu, G. C.-K.; Sanderson, R. J.; Vernstrom, G.; Stevens, D. A.; Atanasoski, R. T.; Debe, M. K.; Dahn, J. R. *J. Electrochem. Soc.* **2010**, *157*, B207.

(211) Liu, G. C.-K.; Stevens, D. A.; Burns, J. C.; Sanderson, R. J.; Vernstrom, G.; Atanasoski, R. T.; Debe, M. K.; Dahn, J. R. *J. Electrochem. Soc.* **2011**, *158*, B919.

(212) Stevens, D. A.; Mehrotra, R.; Sanderson, R. J.; Vernstrom, G. D.; Atanasoski, R. T.; Debe, M. K.; Dahn, J. R. *J. Electrochem. Soc.* **2011**, *158*, B905.

(213) Stevens, D. A.; Wang, S.; Sanderson, R. J.; Liu, G. C. K.; Vernstrom, G. D.; Atanasoski, R. T.; Debe, M. K.; Dahn, J. R. *J. Electrochem. Soc.* **2011**, *158*, B899.

(214) Bonakdarpour, A.; Lobel, R.; Atanasoski, R. T.; Vernstrom, G. D.; Schmoeckel, A. K.; Debe, M. K.; Dahn, J. R. *J. Electrochem. Soc.* **2006**, *153*, A1835.

(215) Mark, K. D.; Radoslav, T. A.; Andrew, J. S. *ECS Transactions* **2011**, *41*, 937.

(216) Stevens, D. A.; Mehrotra, R.; Sanderson, R. J.; Vernstrom, G. D.; Atanasoski, R. T.; Debe, M. K.; Dahn, J. R. *J. Electrochem. Soc.* **2011**, *158*, B905.

(217) Tritsaris, G. A.; Norskov, J. K.; Rossmeisl, J. *Electrochim. Acta* **2011**, *56*, 9783.

(218) Gago, A. S.; Morales-Acosta, D.; Arriaga, L. G.; Alonso-Vante, N. *J. Power Sources* **2011**, *196*, 1324.

(219) Feng, Y.; Gago, A.; Timperman, L.; Alonso-Vante, N. *Electrochim. Acta* **2011**, *56*, 1009.

(220) Feng, Y.; He, T.; Alonso-Vante, N. *Chem. Mater.* **2008**, *20*, 26.

(221) Schmidt, T. J.; Paulus, U. A.; Gasteiger, H. A.; Alonso-Vante, N.; Behm, R. J. *J. Electrochem. Soc.* **2000**, *147*, 2620.

(222) Feng, Y. J.; He, T.; Alonso-Vante, N. *Fuel Cells* **2010**, *10*, 77.

(223) Hu, Z.; Chen, C.; Meng, H.; Wang, R.; Shen, P. K.; Fu, H. *Electrochem. Commun.* **2011**, *13*, 763.

(224) Lee, K. C.; Ishihara, A.; Mitsushima, S.; Kamiya, N.; Ota, K. I. *Electrochim. Acta* **2004**, *49*, 3479.

(225) Vossen, A.; McIntyre, D. R.; Burstein, G. T. Direct Methanol Fuel Cells. *Proceedings of the International Symposium, Electrochemical Society Proceedings*, 2001; Vol. *2001−4*.

(226) Voinov, M.; Buhler, D.; Tannenbe., H. *J. Electrochem. Soc.* **1971**, *118*, 1137.

(227) Liu, G.; Zhang, H. M.; Wang, M. R.; Zhong, H. X.; Chen, J. *J. Power Sources* **2007**, *172*, 503.

(228) Maekawa, Y.; Ishihara, A.; Kim, J.-H.; Mitsushima, S.; Ota, K.-i. *Electrochem. Solid State Lett.* **2008**, *11*, B109.

(229) Meng, H.; Larouche, N.; Lefevre, M.; Jaouen, F.; Stansfield, B.; Dodelet, J.-P. *Electrochim. Acta* **2010**, *55*, 6450.

(230) Charreteur, F.; Jaouen, F. d. r.; Dodelet, J.-P. *Electrochim. Acta* **2009**, *54*, 6622.

(231) Faubert, G.; Cote, R.; Guay, D.; Dodelet, J. P.; Denes, G.; Poleunis, C.; Bertrand, P. *Electrochim. Acta* **1998**, *43*, 1969.

(232) Faubert, G.; Cote, R.; Dodelet, J. P.; Lefevre, M.; Bertrand, P. *Electrochim. Acta* **1999**, *44*, 2589.

(233) Faubert, G.; Lalande, G.; Cote, R.; Guay, D.; Dodelet, J. P.; Weng, L. T.; Bertrand, P.; Denes, G. *Electrochim. Acta* **1996**, *41*, 1689.

(234) Meng, H.; Jaouen, F.; Proietti, E.; Lefevre, M.; Dodelet, J.-P. *Electrochem. Commun.* **2009**, *11*, 1986.

(235) Qu, L.; Liu, Y.; Baek, J.-B.; Dai, L. *ACS Nano* **2010**, *4*, 1321.

(236) Lee, K. R.; Lee, K. U.; Lee, J. W.; Ahn, B. T.; Woo, S. I. *Electrochem. Commun.* **2010**, *12*, 1052.

(237) Zhang, L.; Xia, Z. *J. Phys. Chem. C* **2011**, *115*, 11170.

(238) Kruusenberg, I.; Alexeyeva, N.; Tammeveski, K.; Kozlova, J.; Matisen, L.; Sammelselg, V.; Solla-Gullon, J.; Feliu, J. M. *Carbon* **2011**, *49*, 4031.

(239) Ayala, P.; Arenal, R.; Rammeli, M.; Rubio, A.; Pichler, T. *Carbon* **2010**, *48*, 575.

(240) Hasche, F.; Oezaslan, M.; Strasser, P. *Phys. Chem. Chem. Phys.* **2010**, *12*, 15251.

(241) Baresel, D.; Sarholz, W.; Scharner, P.; Schmitz, J. *Ber. Bunsen-Ges.* **1974**, *78*, 608.

(242) Fischer, C.; Alonso-Vante, N.; Fiechter, S.; Tributsch, H. *J. Appl. Electrochem.* **1995**, *25*, 1004.

(243) Gotoh, Y.; Yamaguchi, I.; Takahashi, Y.; Akimoto, J.; Goto, M.; Kawaguchi, K.; Yamamoto, N.; Onoda, M. *Solid State Ionics* **2004**, *172*, 519.

(244) Tanigaki, T.; Saito, Y.; Nakada, T.; Tsuda, N.; Kaito, C. *J. Nanopart. Res.* **2002**, *4*, 83.

(245) Gleizes, A. N. *Chem. Vap. Deposition* **2000**, *6*, 155.

(246) Bochmann, M. *Chem. Vap. Deposition* **1996**, *2*, 85.

(247) Kristl, M.; Drofenik, M. *Ultrason. Sonochem.* **2008**, *15*, 695.

(248) Li, K.; Liu, X.; Wang, H.; Yan, H. *Mater. Lett.* **2006**, *60*, 3038.

(249) Ohtani, T.; Araki, M.; Shohno, M. *Solid State Ionics* **2004**, *172*, 197.

(250) Qing, L.; Yi, D.; Mingwang, S.; Ji, W.; Guihua, Y.; Yitai, Q. *Mater. Res. Bull.* **2003**, 38.

(251) Harpeness, R.; Palchik, O.; Gedanken, A.; Palchik, V.; Amiel, S.; Slifkin, M. A.; Weiss, A. M. *Chem. Mater.* **2002**, *14*, 2094.

(252) Li, B.; Xie, Y.; Huang, J.; Qian, Y. *Ultrason. Sonochem.* **1999**, *6*, 217.

(253) Liang, S.; Yeming, X.; Quan, L. *Solid State Commun.* **2008**, 146.

(254) Ji, H. M.; Cao, J. M.; Feng, J.; Chang, X.; Ma, X. J.; Liu, J. S.; Zheng, M. B. *Mater. Lett.* **2005**, *59*, 3169.

(255) Qi, L.; Ni, Y. H.; Gui, Y.; Hong, J. M.; Zheng, X. *Mater. Chem. Phys.* **2005**, *89*, 379.

(256) Salavati-Niasari, M.; Bazarganipour, M.; Davar, F.; Fazl, A. A. *Appl. Surf. Sci.* **2010**, *257*, 781.

(257) Khanna, P. K.; Rao, K. S.; Patil, K. R.; Singh, V. N.; Mehta, B. R. *J. Nanopart. Res.* **2010**, *12*, 101.

(258) Du, W.; Qian, X.; Yin, J.; Gong, Q. *Chem.—Eur. J.* **2007**, *13*, 8840.

(259) Yuan, B.; Luan, W.; Tu, S.-T. *Dalton Trans. (Cambridge)* **2011**, *41*, 772.

(260) Wang, D.-W.; Wang, Q.-H.; Wang, T.-M. *CrystEngComm* **2009**, *12*, 755.

(261) Zhang, Y. C.; Qiao, T.; Hu, X. Y.; Zhou, W. D. *Mater. Res. Bull.* **2005**, *40*, 1696.

(262) Gautam, U. K.; Seshadri, R. *Mater. Res. Bull.* **2004**, *39*, 669.

(263) Yang, J.; Cheng, G. H.; Zeng, J. H.; Yu, S. H.; Liu, X. M.; Qian, Y. T. *Chem. Mater.* **2001**, *13*, 848.

(264) Li, J.; Chen, Z.; Wang, R. J.; Proserpio, D. M. *Coord. Chem. Rev.* **1999**, *192*, 707.

(265) Susac, D.; Zhu, L.; Teo, M.; Sode, A.; Wong, K. C.; Wong, P. C.; Parsons, R. R.; Bizzotto, D.; Mitchell, K. A. R.; Campbell, S. A. *J. Phys. Chem. C* **2007**, *111*, 18715.

(266) Zhu, L.; Susac, D.; Lam, A.; Teo, M.; Wong, P. C.; Bizzotto, D.; Campbell, S. A.; Parsons, R. R.; Mitchell, K. A. R. *J. Solid State Chem.* **2006**, *179*, 3942.

(267) Teo, M.; Wong, P. C.; Zhu, L.; Susac, D.; Campbell, S. A.; Mitchell, K. A. R.; Parsons, R. R.; Bizzotto, D. *Appl. Surf. Sci.* **2006**, *253*, 1130.

(268) Susac, D.; Sode, A.; Zhu, L.; Wong, P. C.; Teo, M.; Bizzotto, D.; Mitchell, K. A. R.; Parsons, R. R.; Campbell, S. A. *J. Phys. Chem. B* **2006**, *110*, 10762.

(269) Feng, Y.; He, T.; Alonso-Vante, N. *Electrochim. Acta* **2009**, *54*, 5252.

(270) Gochi-Ponce, Y.; Alonso-Nunez, G.; Alonso-Vante, N. *Electrochem. Commun.* **2006**, *8*, 1487.

(271) Alonso-Vante, N.; Bogdanoff, P.; Tributsch, H. *J. Catal.* **2000**, *190*, 240.

(272) Liu, R.; Wu, D.; Feng, X.; Müllen, K. *Angew. Chem., Int. Ed.* **2010**, *49*, 2565.

(273) Gong, K.; Du, F.; Xia, Z.; Durstock, M.; Dai, L. *Science* **2009**, *323*, 760.

(274) Kruusenberg, I.; Alexeyeva, N.; Tammeveski, K. *Carbon* **2009**, *47*, 651.

(275) Alexeyeva, N.; Shulga, E.; Kisand, V.; Kink, I.; Tammeveski, K. *J. Electroanal. Chem.* **2007**, *648*, 169.

(276) Subramanian, N. P.; Li, X.; Nallathambi, V.; Kumaraguru, S. P.; Colon-Mercado, H.; Wu, G.; Lee, J.-W.; Popov, B. N. *J. Power Sources* **2009**, *188*, 38.

(277) Terrones, M.; Ajayan, P. M.; Banhart, F.; Blase, X.; Carroll, D. L.; Charlier, J. C.; Czerw, R.; Foley, B.; Grobert, N.; Kamalakaran, R.; Kohler-Redlich, P.; Rühle, M.; Seeger, T.; Terrones, H. *Appl. Phys. A: Mater. Sci. Process.* **2002**, *74*, 355.

(278) Ozaki, J.-i.; Tanifuji, S.-i.; Furuichi, A.; Yabutsuka, K. *Electrochim. Acta* **2010**, *55*, 1864.

(279) Biddinger, E. J.; Ozkan, U. S. *J. Phys. Chem. C* **2010**, *114*, 15306.

(280) Liang, Y.; Li, Y.; Wang, H.; Zhou, J.; Wang, J.; Regier, T.; Dai, H. *Nat. Mater.* **2011**, *10*, 780.

(281) Chen, P.; Xiao, T.-Y.; Li, H.-H.; Yang, J.-J.; Wang, Z.; Yao, H.-B.; Yu, S.-H. *ACS Nano* **2012**, *6*, 712−719.

(282) Jasinski, R. *Nature* **1964**, *201*, 1212.

(283) Jasinski, R. *J. Electrochem. Soc.* **1965**, *112*, 526.

(284) Bashyam, R.; Zelenay, P. *Nature* **2006**, *443*, 63.

(285) Zagal, J. H.; Griveau, S.; Francisco Silva, J.; Nyokong, T.; Bedioui, F. *Coord. Chem. Rev.* **2010**, *254*, 2755.

(286) Zagal, J. H.; Griveau, S.; Ozoemena, K. I.; Nyokong, T.; Bedioui, F. *J. Nanosci. Nanotechnol.* **2009**, *9*, 2201.

(287) Jaouen, F.; Charreteur, F.; Dodelet, J. P. *J. Electrochem. Soc.* **2006**, *153*, A689.

(288) Villers, D.; Jacques-Bedard, X.; Dodelet, J. P. *J. Electrochem. Soc.* **2004**, *151*, A1507.

(289) Jaouen, F.; Marcotte, S.; Dodelet, J. P.; Lindbergh, G. *J. Phys. Chem. B* **2003**, *107*, 1376.

(290) Lefevre, M.; Dodelet, J. P.; Bertrand, P. *J. Phys. Chem. B* **2000**, *104*, 11238.

(291) Gupta, S. L.; Tryk, D.; Daroux, M.; Aldred, W.; Yeager, E. *J. Electrochem. Soc.* **1986**, *133*, C120.

(292) Scherson, D.; Tanaka, A. A.; Gupta, S. L.; Tryk, D.; Fierro, C.; Holze, R.; Yeager, E. B.; Lattimer, R. P. *Electrochim. Acta* **1986**, *31*, 1247.

(293) Hossain, M. S.; Tryk, D.; Yeager, E. *Electrochim. Acta* **1989**, *34*, 1733.

(294) Marcotte, S.; Villers, D.; Guillet, N.; Roue, L.; Dodelet, J. P. *Electrochim. Acta* **2004**, *50*, 179.

(295) Herranz, J.; Jaouen, F.; Lefevre, M.; Kramm, U. I.; Proietti, E.; Dodelet, J.-P.; Bogdanoff, P.; Fiechter, S.; Abs-Wurmbach, I.; Bertrand, P.; Arruda, T. M.; Mukerjee, S. *J. Phys. Chem. C* **2011**, *115*, 16087.

(296) Jaouen, F.; Proietti, E.; Lefevre, M.; Chenitz, R.; Dodelet, J.-P.; Wu, G.; Chung, H. T.; Johnston, C. M.; Zelenay, P. *Energy Environ. Sci.* **2010**, *4*, 114.

(297) Tian, J.; Birry, L.; Jaouen, F.; Dodelet, J. P. *Electrochim. Acta* **2011**, *56*, 3276.

(298) Charreteur, F.; Jaouen, F.; Ruggeri, S.; Dodelet, J.-P. *Electrochim. Acta* **2008**, *53*, 2925.

(299) Proietti, E.; Ruggeri, S.; Dodelet, J.-P. *J. Electrochem. Soc.* **2008**, *155*, B340.

(300) Charreteur, F.; Jaouen, F.; Dodelet, J.-P. *Electrochim. Acta* **2009**, *54*, 6622.

(301) Jaouen, F.; Dodelet, J.-P. *J. Phys. Chem. C* **2009**, *113*, 15422.

(302) Lefevre, M.; Proietti, E.; Jaouen, F.; Dodelet, J.-P. *Science* **2009**, *324*, 71.

(303) Lefevre, M.; Dodelet, J. P.; Bertrand, P. *J. Phys. Chem. B* **2002**, *106*, 8705.

(304) Lefevre, M.; Dodelet, J. P. *Electrochim. Acta* **2003**, *48*, 2749.

(305) Wu, G.; More, K. L.; Johnston, C. M.; Zelenay, P. *Science* **2011**, *332*, 443.

(306) Shi, Z.; Liu, H.; Lee, K.; Dy, E.; Chlistunoff, J.; Blair, M.; Zelenay, P.; Zhang, J.; Liu, Z.-S. *J. Phys. Chem. C* **2011**, *115*, 16672.

(307) Wu, G.; Johnston, C. M.; Mack, N. H.; Artyushkova, K.; Ferrandon, M.; Nelson, M.; Lezama-Pacheco, J. S.; Conradson, S. D.; More, K. L.; Myers, D. J.; Zelenay, P. *J. Mater. Chem.* **2011**, *21*, 11392.

(308) Gasteiger, H. A.; Kocha, S. S.; Sompalli, B.; Wagner, F. T. *Appl. Catal., B* **2005**, *56*, 9.

(309) Gasteiger, H. A.; Panels, J. E.; Yan, S. G. *J. Power Sources* **2004**, *127*, 162.

(310) Linse, N.; Gubler, L.; Scherer, G. G.; Wokaun, A. *Electrochim. Acta* **2011**, *56*, 7541.

(311) Linse, N.; Scherer, G. G.; Wokaun, A.; Gubler, L. Start/Stop Induced Carbon Corrosion in Polymer Electrolyte Fuel Cells. In *Proceedings of the Asme 8th International Conference on Fuel Cell Science, Engineering, and Technology*; 2010; Vol. 2, p 357.

(312) Schuler, G. A. *Dissertation ETH Zürich No. 18883*, 2012; p 27.

(313) Greszler, T. A.; Moylan, T. E.; Gasteiger, H. A. Modeling the Impact of Cation Contamination in a Polymer Electrolyte Membrane Fuel Cell. In *Handbook of Fuels−Fundamentals, Technology and Applications*; Vielstich, W., Yokokawa, H., Gasteiger, H. A., Eds.; John Wiley & Sons: New York, 2009; Vol. 6; p 728.

(314) SKW. Stickstoffwerke Piesteritz GmbH, Personal Communication, 2010.

(315) Ham, D. J.; Lee, J. S. *Energies* **2009**, *2*, 873.

(316) Antolini, E.; Gonzalez, E. R. *Solid State Ionics* **2009**, *180*, 746.

(317) Levy, R. B.; Boudart, M. *Science* **1973**, *181*, 547.

(318) Christian, J. B.; Smith, S; Whittingham, M. S.; Abruna, H. D. *Electrochem. Commun.* **2007**, *9*, 2128.

(319) Antolini, E.; Gonzalez, E. R. *Appl. Catal., B* **2010**, *96*, 245.

(320) Guofeng, C.; Pei Kang, S.; Hui, M.; Jie, Z.; Gang, W. *J. Power Sources* **2011**, *196*.

(321) Houston, J. E.; Laramore, G. E.; Park, R. L. *Science* **1974**, *185*, 258.

(322) Cui, G.; Shen, P. K.; Meng, H.; Zhao, J.; Wu, G. *J. Power Sources* **2011**, *196*, 6125.

(323) Chhina, H.; Campbell, S.; Kesler, O. *J. Power Sources* **2007**, *164*, 431.

(324) Ota, K.; Ishihara, A.; Mitsushima, S.; Lee, K.; Suzuki, Y.; Horibe, N.; Nakagawa, T.; Kamiya, N. *J. New Mater. Electrochem. Syst.* **2005**, *8*, 25.

(325) Chhina, H.; Campbell, S.; Kesler, O. *J. Power Sources* **2008**, *179*, 50.

(326) d'Arbigny, J. B.; Taillades, G.; Marrony, M.; Jones, D. J.; Roziere, J. *Chem. Commun.* **2011**, *47*, 7950.

(327) Sasaki, K.; Takasaki, F.; Noda, Z.; Hayashi, S.; Shiratori, Y.; Ito, K. *ECS Trans.* **2010**, *33*, 473.

(328) Kim, J.-H.; Ishihara, A.; Mitsushima, S.; Kamiya, N.; Ota, K.-I. *Electrochim. Acta* **2007**, *52*, 2492.

(329) Liu, Y.; Ishihara, A.; Mitsushima, S.; Kamiya, N.; Ota, K.-i. *J. Electrochem. Soc.* **2007**, *154*, B664.

(330) Huang, S.-Y.; Ganesan, P.; Popov, B. N. *Appl. Catal., B* **2010**, *96*, 224.

(331) Masao, A.; Noda, S.; Takasaki, F.; Ito, K.; Sasaki, K. *Electrochem. Solid State Lett.* **2009**, *12*, B119.

(332) Matsui, T.; Fujiwara, K.; Okanishi, T.; Kikuchi, R.; Takeguchi, T.; Eguchi, K. *J. Power Sources* **2006**, *155*, 152.

(333) Wesselmark, M.; Wickman, B.; Lagergren, C.; Lindbergh, G. *Electrochim. Acta* **2009**, *55*, 7590.

(334) Chhina, H.; Campbell, S.; Kesler, O. *J. Electrochem. Soc.* **2007**, *154*, B533.

(335) Wickman, B.; Wesselmark, M.; Lagergren, C.; Lindbergh, G. *Electrochim. Acta* **2011**, *56*, 9496.

(336) Takasu, Y.; Suzuki, M.; Yang, H.; Ohashi, T.; Sugimoto, W. *Electrochim. Acta* **2009**, *55*, 8220.

(337) Ishihara, A.; Tamura, M.; Maekawa, Y.; Ohgi, Y.; Matsuzawa, K.; Mitsushima, S.; Ota, K. Group 4 and 5 Oxide-Based Compounds as New Cathodes without Platinum Group Metals for PEFC. In *Proton Exchange Membrane Fuel Cells 8, Parts 1 and 2*, **2008**; Vol. 16; p 449.

(338) Yan, L.; Ishihara, A.; Mitsushima, S.; Kamiya, N.; Ota, K. *Electrochem. Solid-State Lett.* **2005**, *8*.

(339) Liu, Y.; Ishihara, A.; Mitsushima, S.; Ota, K.-i. *Electrochim. Acta* **2010**, *55*, 1239.

(340) Ishihara, A.; Doi, S.; Mitsushima, S.; Ota, K.-i. *Electrochim. Acta* **2008**, *53*, 5442.

(341) Chisaka, M.; Iijima, T.; Yaguchi, T.; Sakurai, Y. *Electrochim. Acta* **2011**, *56*, 4581.

(342) Chisaka, M.; Suzuki, Y.; Iijima, T.; Sakurai, Y. *J. Phys. Chem. C* **2011**, *115*, 20610.

(343) Ishihara, A.; Ohgi, Y.; Matsuzawa, K.; Mitsushima, S.; Ota, K.-i. *Electrochim. Acta* **2010**, *55*, 8005.

(344) Okanishi, T.; Matsui, T.; Takeguchi, T.; Kikuchi, R.; Eguchi, K. *Appl. Catal., A* **2006**, *298*, 181.

(345) Lewera, A.; Timperman, L.; Roguska, A.; Alonso-Vante, N. *J. Phys. Chem. C* **2011**, *115*, 20153.

(346) Timperman, L.; Feng, Y. J.; Vogel, W.; Alonso-Vante, N. *Electrochim. Acta* **2009**, *55*, 7558.

(347) Guerin, S.; Hayden, B. E.; Pletcher, D.; Rendall, M. E.; Suchsland, J.-P. *J. Comb. Chem.* **2006**, *8*, 679.

(348) Hayden, B. E.; Pletcher, D.; Suchsland, J.-P.; Williams, L. *J. Phys. Chem. Chem. Phys.* **2009**, *11*, 1564.

(349) Hayden, B. E.; Pletcher, D.; Suchsland, J.-P.; Williams, L. *J. Phys. Chem. Chem. Phys.* **2009**, *11*, 9141.

(350) Ligthart, D.; van Santen, R. A.; Hensen, E. J. M. *J. Catal.* **2011**, *280*, 206.

(351) Sasaki, K.; Zhang, L.; Adzic, R. R. *Phys. Chem. Chem. Phys.* **2008**, *10*, 159.

(352) Van, T. T. H.; Pillai, K. C.; Chou, H. L.; Pan, C. J.; Rick, J.; Su, W. N.; Hwang, B. J.; Lee, J. F.; Sheu, H. S.; Chuang, W. T. *Energy Environ. Sci.* **2011**, *4*, 4194.

(353) Subban, C.; Zhou, Q.; Leonard, B.; Ranjan, C.; Edvenson, H. M.; DiSalvo, F. J.; Munie, S.; Hunting, J. *Philos. Trans. R. Soc., A* **2010**, *368*, 3243.

(354) Wang, D.; Subban, C. V.; Wang, H.; Rus, E.; DiSalvo, F. J.; Abruna, H. D. *J. Am. Chem. Soc.* **2010**, *132*, 10218.

(355) Ho, V. T. T.; Pan, C.-J.; Rick, J.; Su, W.-N.; Hwang, B.-J. *J. Am. Chem. Soc.* **2011**, *133*, 11716.

(356) Zhang, H.; Wang, Y.; Fachini, E. R.; Cabrera, C. R. *Electrochem. Solid-State Lett.* **1999**, *2*, 437.

(357) Huang, S.-Y.; Ganesan, P.; Park, S.; Popov, B. N. *J. Am. Chem. Soc.* **2009**, *131*, 13898.

(358) Sine, G.; Foti, G.; Comninellis, C. *J. Electroanal. Chem.* **2006**, *595*, 115.

(359) Panizza, M.; Cerisola, G. *Electrochim. Acta* **2005**, *51*, 191.

(360) Compton, R. G.; Foord, J. S.; Marken, F. *Electroanalysis* **2003**, *15*, 1349.

(361) Moore, A.; Celorrio, V.; de Oca, M. M.; Plana, D.; Hongthani, W.; Lazaro, M. J.; Fermin, D. J. *Chem. Commun.* **2011**, *47*, 7656.

(362) Hongthani, W.; Fox, N. A.; Fermin, D. J. *Langmuir* **2011**, *27*, 5112.

(363) Schmidt, T. J. *ECS Trans.* **2012**, *45*, 3.